

**A NEAR OPTIMUM STRATEGY FOR SEMIPASSIVE ATTITUDE CONTROL OF LARGE
COMMUNICATIONS SATELLITES**

by

PREM KUMAR LAKSHMANAN

B.Tech.(Hons), Banaras Hindu University, 1982

**A THESIS SUBMITTED IN PARTIAL FULFILMENT OF
THE REQUIREMENTS FOR THE DEGREE OF
MASTER OF APPLIED SCIENCE**

in

**THE FACULTY OF GRADUATE STUDIES
Department of Mechanical Engineering**

**We accept this thesis as conforming
to the required standard**

THE UNIVERSITY OF BRITISH COLUMBIA

May 1985

© **PREM KUMAR LAKSHMANAN, 1985**

In presenting this thesis in partial fulfilment of the requirements for an advanced degree at the University of British Columbia, I agree that the Library shall make it freely available for reference and study. I further agree that permission for extensive copying of this thesis for scholarly purposes may be granted by the head of my department or by his or her representatives. It is understood that copying or publication of this thesis for financial gain shall not be allowed without my written permission.

Department of Mechanical Engineering

The University of British Columbia
1956 Main Mall
Vancouver, Canada
V6T 1Y3

Date 23 May 1985

ABSTRACT

Effectiveness of solar radiation pressure in the three-axis attitude control of present day and next generation of large communications satellites is investigated. A simple two-flap configuration is used with optimization of the direction of the applied control moment rather than the magnitude of the weak solar radiation pressure. Simulations were carried out in the presence of varying orbital eccentricity and inclination, solar aspect angle and controller dynamics parameters. Time histories of librational response against orbital position are presented for controlled and uncontrolled conditions. The results suggest the semipassive controller to be quite effective over a wide range of system parameters and it can meet the exacting pointing accuracy demanded by large communications satellites.

ACKNOWLEDGEMENT

The author wishes to express his deepest gratitude to Professor V.J. Modi for his patience, time and effort throughout the course of the research programme and during the preparation of this thesis. His guidance and encouragement have been invaluable.

Special thanks are due to W.H.H.J. Lunscher, from the Department of Electrical Engineering, for his help in the incipient stages of this project. Thanks are also due to my fellow graduate students for discussions and advice.

The investigation reported here was supported by the Natural Sciences and Engineering Research Council of Canada, Grant No. A-2181.

Table of Contents

ABSTRACT	ii
ACKNOWLEDGEMENT	iii
LIST OF FIGURES	vi
LIST OF TABLES	viii
NOMENCLATURE	ix
1. INTRODUCTION	1
1.1 Preliminary Remarks	1
1.2 A Brief Review of Literature	5
1.3 Scope of the Present Investigation	6
2. FORMULATION OF THE DYNAMICAL PROBLEM	10
2.1 Kinematics of the System	10
2.2 Evaluation of the Energy Expressions	13
2.3 Nonconservative Forces and Constants of Motion	14
2.4 Equations of Motion	15
3. CONTROLLER CONFIGURATION AND GENERALIZED FORCES	18
3.1 Description of the Controller	18
3.2 Evaluation of the Solar Radiation Pressure Force	18
3.3 Determination of the Controller Plate Orientation	21
3.4 Position of the Centre of Pressure in Principal Coordinates	23
3.5 Evaluation of the Controller Plate Moments and Generalized Forces	24
4. CONTROL PHILOSOPHY AND OPTIMIZATION OF GENERALIZED FORCES	28
4.1 Introduction	28
4.2 Constraints of the Problem	29
4.3 The Constraint Surface	31
4.4 Unconstrained Minimization	32
4.5 Some Further Remarks	35

4.6 Nature of the Controller Moments and Practical Feasibility of the Controller	36
5. CONTROL STRATEGY	40
5.1 Nature and Objective of the Control Strategy	40
5.2 Alignment Control	46
5.3 θ_S, θ_R Equalization Control	50
5.4 Pitch Control During Momentum Alignment	51
5.5 Total Applied Moment	54
5.6 Final Pitch Alignment	54
5.7 Arbitrary Orientation in Space	56
6. RESULTS AND DISCUSSIONS	59
7. CONCLUDING REMARKS	70
LIST OF REFERENCES	71
APPENDIX A: EVALUATION OF $g_{1x} \Big _{\epsilon=0}$	74
APPENDIX B: CONTROL MOMENT SYMMETRIES	77
APPENDIX C: BANG-BANG COMPENSATION	80

LIST OF FIGURES

		Page
Figure 1.1	Variation of environmental torques with altitude for a representative satellite	3
Figure 1.2	Geometry of recently launched India's multipurpose communications satellite INSAT 1-A	7
Figure 1.3	Geometry of the proposed European Space Agency's communications satellite L-SAT 1	9
Figure 2.1	Geometry of motion of an axisymmetric satellite in the solar pressure environment	11
Figure 3.1	Geometry of the proposed controller	19
Figure 3.2	Orientation of a plate element and solar pressure force components	20
Figure 4.1	Maximum controller moment surfaces under varying solar elevation angle	37
Figure 5.1	Relative geometry of the axis of symmetry, the angular momentum vector and the reference momentum vector	42
Figure 5.2	Control Strategy flow chart for equilibrium configuration as final orientation	45
Figure 6.1	Librational response of INSAT 1-A to a representative impulsive disturbance in an ecliptic orbit in the uncontrolled mode and in orbits of varying inclinations in the controlled mode	62
Figure 6.2	Librational response of L-SAT 1 to a representative impulsive disturbance in an ecliptic orbit in the uncontrolled mode and in orbits of varying inclinations in the controlled mode	63
Figure 6.3	Effectiveness of the near-optimal solar pressure control strategy on INSAT 1-A for elliptic orbits	64
Figure 6.4	Influence of varying orbit eccentricities on the controlled librational response of L-SAT 1	65
Figure 6.5	Effect of solar aspect angle on the attitude motion of INSAT 1-A with the solar pressure controller	66

Figure 6.6	Influence of varying solar aspect angles on the librational response of L-SAT 1 in the presence of the solar pressure controller	67
Figure 6.7	Effect of changes in the controller dynamics parameter on the librational response	68
Figure 6.8	Plot showing versatility of the solar pressure controller in undertaking large angle slewing maneuvers	69

LIST OF TABLES

	Page
Table 5.1 Switch point and moment direction during final pitch alignment	55

NOMENCLATURE

A	control plate area
C	controller dynamics parameter, $2A\rho p_0 R^3 \epsilon / \mu I_{xx}$
$E(\theta)$	$(1+e)^3 / (1+e \cos\theta)^4$
I	inertia parameter of an axisymmetric ($I_{yy} = I_{zz}$) satellite, I_{xx} / I_{yy}
F	cost function, $-\mathbf{N} \cdot \mathbf{N}_d$
$\bar{\mathbf{F}}$	solar radiation pressure force
I_{xx}, I_{yy}, I_{zz}	principal moments of inertia of the satellite
I_{xp}, I_{xr}	moments of inertia of platform and rotor, respectively, about the axis of symmetry
\mathbf{l}_s	unit vector along the axis of symmetry
K	viscous damping parameter, $K_d (R^3 / \mu)^{1/2} / I_{yy}$
K_d	viscous damping coefficient
L	angular momentum vector
L_a	angular momentum of the rotor
L_R	unit vector of the reference angular momentum
N	applied moment
$\left. \begin{matrix} \mathbf{N}_d, \mathbf{N}_{d1} \\ \mathbf{N}_{d2}, \mathbf{N}_{d3} \end{matrix} \right\}$	desired moment vector directions, Figure 5.2
P	pericenter
Q_i	applied generalized moment, $i = \gamma, \beta, \lambda$
R	distance between the pericenter and the center of force
S	center of mass of the satellite
e	orbit eccentricity
g	directional constraint vector
h	distance between the satellite center of mass and the controller arm hinge point

i	inclination of the orbital plane from the ecliptic plane
$\bar{i}, \bar{j}, \bar{k}$	unit vectors along the principal body coordinates x, y, z , respectively
n	vector bisecting the angle between L_R and I_s
\hat{n}	unit vector normal to the controller plate
p_o	solar radiation pressure, 4.65×10^{-6} Pascal
\hat{u}	unit vector in the direction of the Sun, $u_i i + u_j j + u_k k$
u_i	$\cos\phi(\sin\gamma\cos\beta\cos\eta + \sin\beta\sin\eta) + \sin\phi\{\cos i$ $(\sin\gamma\cos\beta\sin\eta - \sin\beta\cos\eta) \sin i \cos\beta\cos\gamma\}$
u_j	$\cos\phi\cos\gamma\cos\eta + \sin\phi(\cos i\cos\gamma\sin\eta + \sin i \sin\gamma)$
u_k	$\cos\phi(\sin\gamma\sin\beta\cos\eta \cos\beta\sin\eta) + \sin\phi\{\cos i$ $(\sin\gamma\sin\beta\sin\eta + \cos\beta\cos\eta) \sin i \sin\beta\cos\gamma\}$
x', y', z'	inertial coordinate system with x normal to the orbital plane and y along the pericenter
x_o, y_o, z_o	rotating coordinate system with x_o normal to the orbital plane and y_o along the local vertical
x_1, y_1, z_1	intermediate and final body coordinates resulting from rotations γ and β about z_o and y_1 axis, respectively
x_2, y_2, z_2	
x, y, z	
$\alpha, \beta, \gamma, \lambda$	rotor I pitch, yaw, roll, and platform II pitch degrees of freedom, respectively
a_1^u, a_2^u	longitude and latitude of the upper and lower plate support arms, respectively
a_1^l, a_2^l	
$\beta_f, \gamma_f, \lambda_f$	final desired attitude
δ^u, δ^l	upper and lower plate rotations, respectively
e	distance between the center of pressure and the controller arm hinge point
θ	true anomaly

η	$\omega + \theta$
$\theta_G, \theta_S, \theta_R$	angle between L_R-I_S , $L-I_S$, and $L-L_R$ planes, respectively
μ	gravitational constant
ξ	angle of incidence of sunlight at the control plate
ρ	reflectivity of the control plate
σ	spin parameter, Equation 2.13
τ	transmissivity of the control plate
ϕ	solar aspect angle
ψ	angle of precession of I_S-L plane about L
$\dot{\psi}$	precession rate of I_S about L in inertial reference
ω	argument of the perigee referred to the ecliptic
ω_x	angular velocity component along the axis of symmetry
ω_y	angular velocity component along y
ω_z	angular velocity component along z

Subscript o indicates initial position. Dots and primes represent differentiation with respect to time and θ , respectively. Bars and boldface letters indicate vectors. Circumflex ($\hat{}$) indicates unit vector.

1. INTRODUCTION

1.1 Preliminary Remarks

Spacecraft motion involves two fundamental areas of interest: the study of the trajectory of its centre of mass, known as orbital mechanics, and the analysis of the motion of the spacecraft about its centre of mass, referred to as attitude dynamics. Orbital mechanics treats the spacecraft as a point mass and is governed by the classical Keplerian relations. Spacecraft, however, have finite dimensions and hence possess inertias. Consideration of the inertias of the spacecraft is necessary to describe its orientation about the centre of mass. The study of motion about the centre of mass, also known as libration, constitutes attitude mechanics.

The simultaneous analysis of coupled orbital and librational motion obviously represents a complex dynamical problem. The analysis involves three coordinates to identify the position of the centre of mass in space and three rotational degrees of freedom to account for the spacecraft's motion about its centre of mass. Fortunately, we have two simplifying factors. Firstly, the Keplerian analysis indicates that orbital motion occurs in a plane. Hence we need only two variables to specify the position of the centre of mass of the satellite in its orbit. Furthermore, it has been observed that for all situations of practical importance, the energy associated with librational motion is merely a small fraction of that contributed by the orbital motion.^{1,2} In other words, the perturbation of the orbital motion by the attitude motion can be neglected. Hence the classical Keplerian relations continue to describe the orbital motion with sufficient accuracy even in the presence of librations, thus decoupling the two motions.

There are numerous situations of practical importance where it is desirable to maintain a satellite in a fixed orientation in space relative to the Earth. Communications satellites with precisely directed antennas, cloud cover scanning

weather satellites, Earth resources survey satellites, scientific and military observations satellites, etc., have preferred orientations dictated by their missions. Unfortunately, despite being precisely oriented at launch, satellites tend to deviate from their desired orientations under the influence of various environmental forces. The dominant among these are:

- (a) local variation of the Earth's gravitational acceleration over the satellite's dimensions (gravity-gradient torque);
- (b) interaction of the ferromagnetic and current carrying materials, on board the satellite, with the Earth's magnetic field (magnetic torque);
- (c) free molecular interaction of the satellite with the Earth's atmosphere (for near-Earth orbits);
- (d) solar radiation pressure acting on reflective surfaces of the exterior of the satellite.

These environmental forces are deterministic and several authors³ have successfully modelled the influence of these forces on the dynamics of spacecraft. By contrast, the less dominant effects of cosmic dust, micrometeorite impacts, solar wind, etc., are random in nature. Brereton⁴ has studied their relative contributions with respect to the specific geometry of the GEOS-A satellite (Figure 1.1). It is of significance to note here that the solar radiation pressure becomes the most dominant environmental torque close to and higher than 36,000 kilometres, which corresponds to the *geosynchronous altitude*, i.e., the altitude at which the satellite's orbital period becomes equal to the Earth's rotational period about its axis.

This raises the possibility of a communications satellite being subjected to a significant solar radiation pressure torque causing large amplitude motion. Obviously, this would be inconsistent with the high pointing accuracy demanded of such satellites. Furthermore, the destabilizing contribution of solar radiation pressure would be magnified in situations where the satellite's projected area to

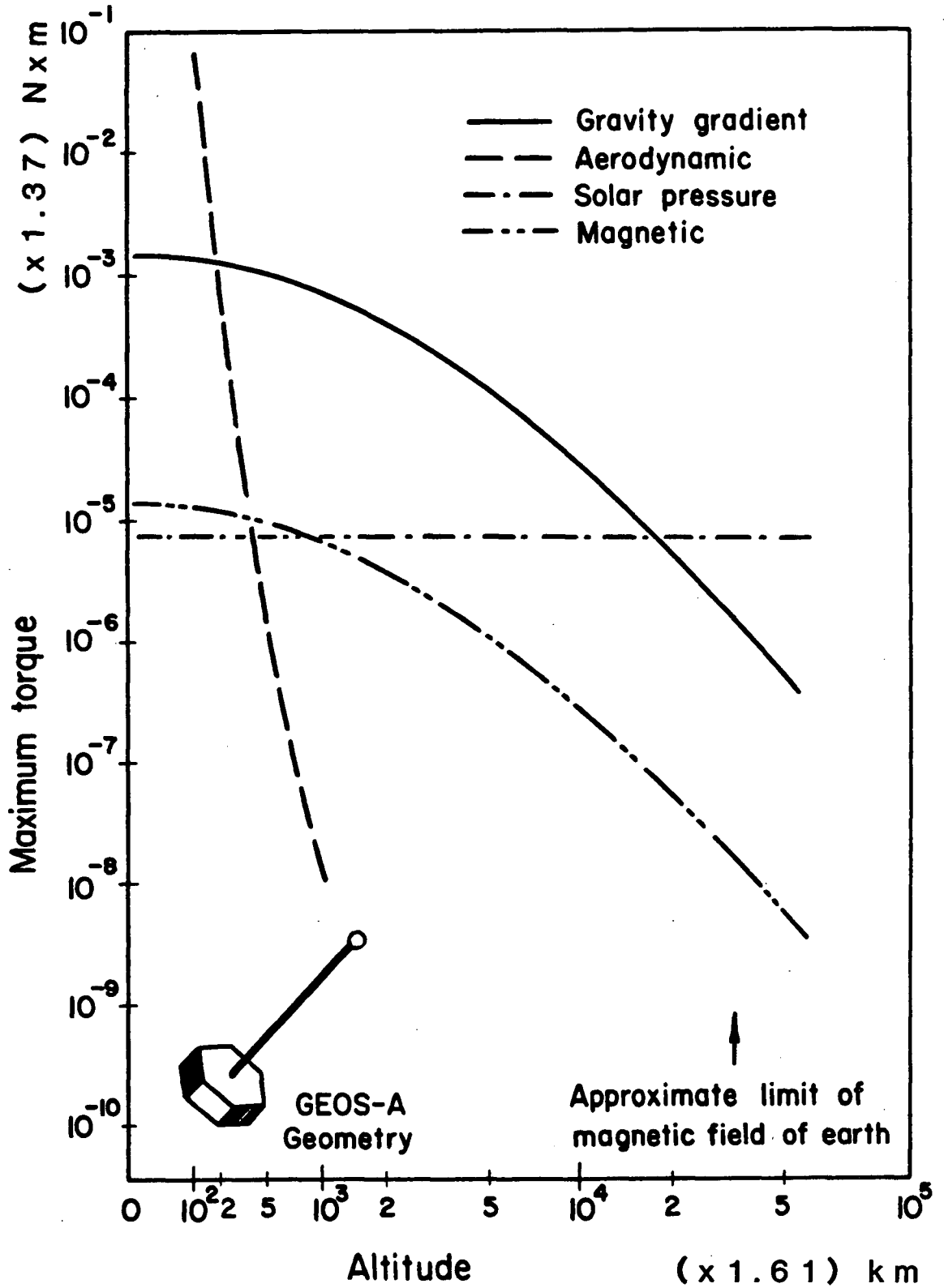


Figure 1.1 Variation of environmental torques with altitude for a representative satellite.

mass ratio becomes relatively large together with an appreciable deviation between the centre of pressure and the centre of mass. Several present day and next generation satellites display these features.

Over the years, a variety of attitude control concepts have been proposed and a few successfully implemented in spacecraft design. They may be classified into major categories as active, passive and semi-passive procedures.

Active stabilization procedures use energy available on board the satellite. Such systems can maintain a specified orientation with almost any desired degree of accuracy at the expense of energy and consequently limit the satellite's useful lifetime. Control systems employing microthrusters, momentum wheels, magnetic coils, etc., belong to this class.

On the other hand, passive stabilization techniques do not rely on the source of energy aboard the satellite. They are characterized by their use of environmental forces to provide the necessary control torques. The approach has proved effective where the orientation requirements are not severe. The Earth's gravity gradient is the most widely exploited environmental force to date.

Semi-passive stabilization systems utilize environmental forces to provide the control effort but at the same time require a small amount of on board power to actuate control mechanisms. The use of normally destabilizing solar torque to advantage in controlling undesirable librations falls in this category. This is achieved through a judicious choice of controller configuration and strategy in conjunction with suitable performance criteria. Such systems are in the developmental stage.

1.2 A Brief Review of Literature

The presence of solar radiation pressure in the space environment has been known for a long time. In 1958, Roberson⁵ estimated its order of magnitude. Utilization of the solar radiation pressure to control satellite motion was first recognized by Garwin⁶ who proposed "solar sailing" as a simple, viable method of propulsion for interplanetary missions. Sohn⁷ considered its application for attitude control using a weather vane type configuration, while Hibbard⁸ suggested the use of a set of reflecting mirrors to increase the available force.

A detailed study of planar librations of a flat plate in an eccentric, ecliptic orbit subjected to the solar, Earth and Earth-reflected radiations is due to Flanagan and Modi^{9,10}.

Modi and Kumar^{11,12} considered the solar radiation pressure acting on a cylindrical satellite and included cross-plane motion in circular orbits. Modi and Pande¹³ studied effects of solar radiation pressure on the attitude dynamics of a slowly spinning system while, Shrivastava and Hablani¹⁴ explored its effect on a gravity stabilized satellite.

Galitiskaya and Kisler¹⁵ analysed a set of panels for three-axis stabilization and qualitatively established their optimum inclinations for the maximum utilization of the solar pressure.

Scull¹⁶ reported an experiment on board Mariner IV where solar radiation pressure had been applied to align the roll-axis of the spacecraft with the Sun-line, on depletion of the attitude control gas. During a major portion of the mission, one of the vanes of the solar controller was inoperative. However, after its subsequent reactivation, the solar controller together with active gyros proved effective in aligning the roll-axis of the spacecraft to within 1° of the Sun-line.

Later Modi and Pande^{17,18} discussed effectiveness of a semi-passive three-axis four plate controller with particular emphasis on simplicity of design and

practical feasibility.

Noting the need for further simplification, Lunscher and Modi¹⁹ improved this controller utilizing a near optimum magnitude independent strategy. A simple two-plate controller was developed that effectively reduced large deviations from equilibrium observed earlier and also shortened the time required to damp disturbances. Through computer simulations, the controller was shown to be quite effective with satellites of relatively small sizes, e.g., **INTELSAT-IV** and **ANIK-I**, having low controller dynamics parameters ($C=2$ and $C=5$, respectively).

1.3 Scope of the Present Investigation

The possibility of stabilizing next generation of large communications satellites using solar radiation pressure through a near optimal three-axis control strategy is explored here. In the beginning, the governing equations of motion for an axisymmetric dual-spin satellite with a stabilized platform undergoing general three dimensional librational motion are derived. This is followed by evaluation of solar radiation pressure induced generalized forces. A two-flap controller having arbitrary orientation in space is described in conjunction with a control strategy which follows the procedure discussed by Modi and Lunscher¹⁹. Finally, the effectiveness of the controller is assessed with reference to the recently launched **INSAT-1A** (Indian National Satellite) and the proposed communications satellite of the European Space Agency, **L-SAT**, to be launched in 1987.

INSAT-1A (Figure 1.2) is a highly advanced communications, direct TV broadcast and meteorological satellite launched in 1982. Its design life was seven years. It had a solar sail mounted on a 12.65 m boom to provide stability against the solar pressure moment due to the deployed solar arrays. Unfortunately, the sail failed to deploy, thus considerably reducing the satellite's useful lifetime. **INSAT-1A**

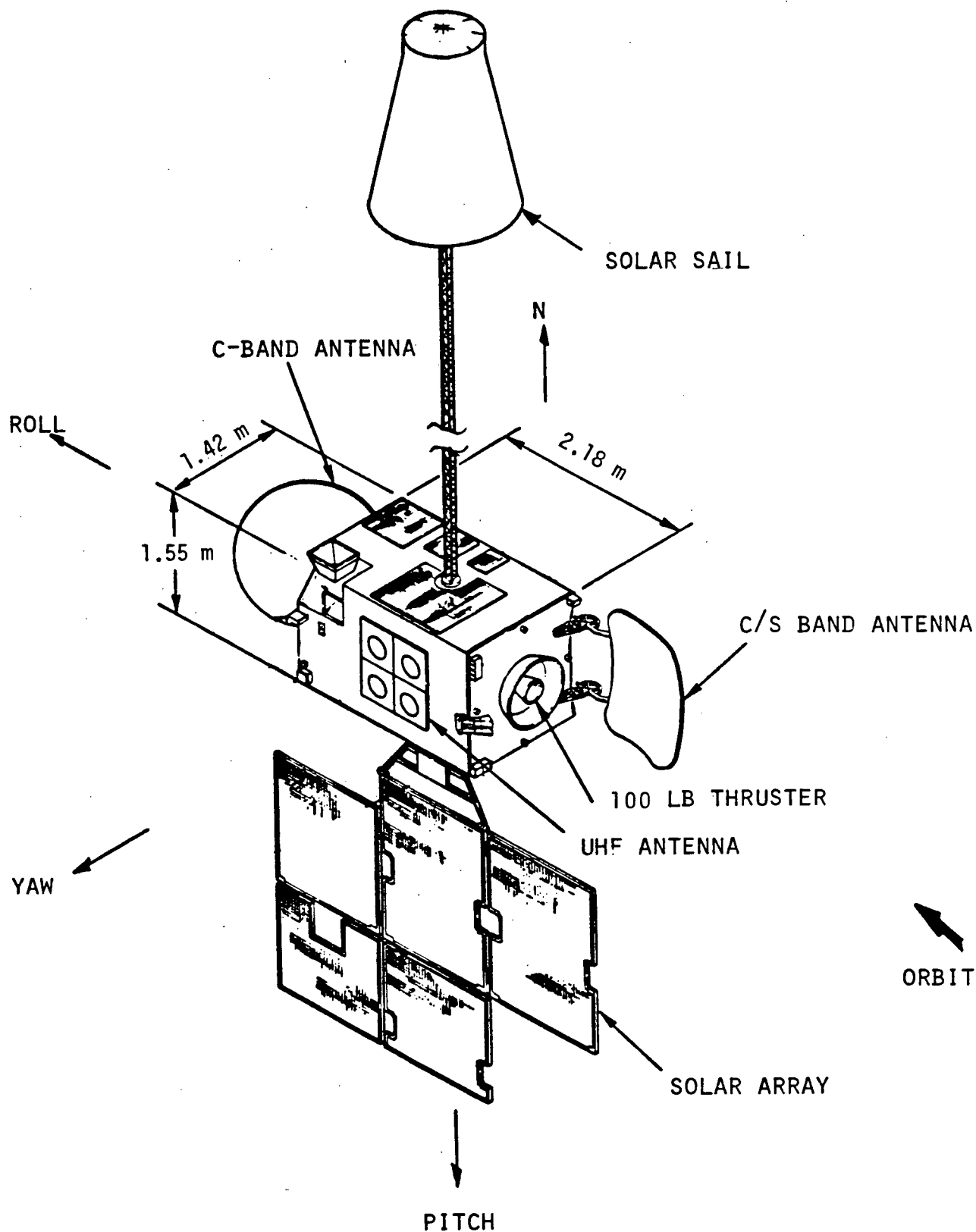


Figure 1.2 Geometry of recently launched India's multipurpose communications satellite INSAT 1-A

dramatically showed the situation in which the solar pressure torque can virtually dictate the librational dynamics. The standby **INSAT-1B**, identical to the failed satellite, was launched in 1983 and is operational. The world is watching with considerable interest the performance of this unique three-in-one multifunctional satellite that promises enormous saving in cost.

The second satellite chosen for study is **L-SAT** (Figure 1.3), a large communications satellite as suggested by its name. It carries two large solar panels spanning a distance of about 33 m, to generate around 7 kW of power. **INSAT-1A** and **L-SAT** have nominal controller dynamics parameters of $C=10$ and $C=80$, respectively.

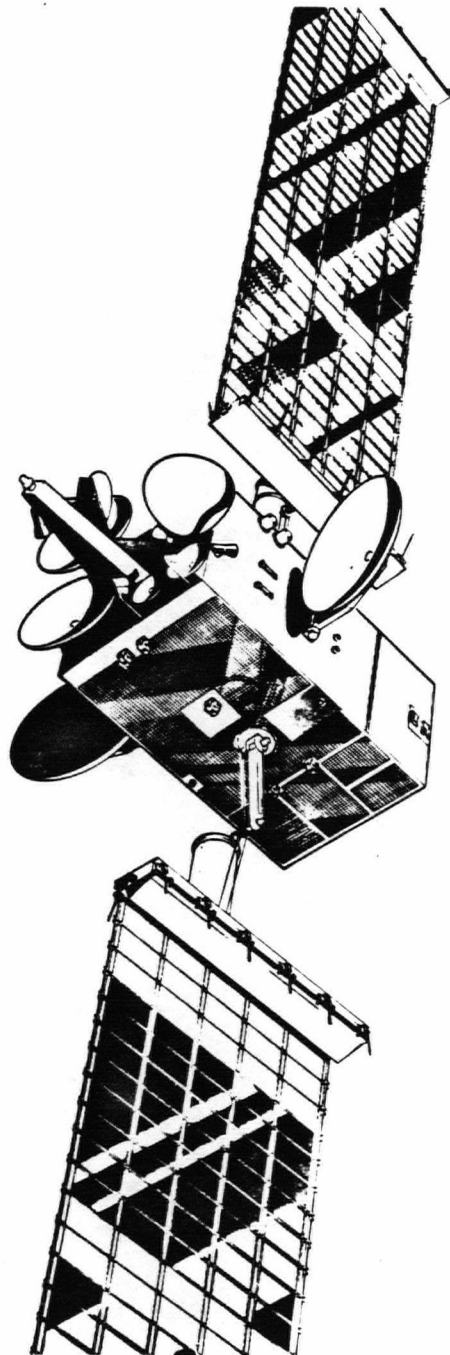


Figure 1.3

Geometry of the proposed
communications satellite L-SAT 1

European Space Agency's

2. FORMULATION OF THE DYNAMICAL PROBLEM

2.1 Kinematics of the System

Consider a dual spin axisymmetric satellite with its centre of mass at S , moving in a Keplerian orbit about the centre of force O , as shown in Figure 2.1. The dual spin satellite consists of a central body I called the rotor, which is spinning at a uniform angular velocity $\dot{\alpha}$, connected to a stabilized platform II. The rotor provides stability through a gyroscopic moment and the platform, despun by control moments, can be used to track a given object in space. Sections I and II are connected through a viscous damper which is effective in the axial direction.

The spatial orientation of the axis of symmetry of the satellite (the x -axis) is completely specified by two successive modified Eulerian rotations γ and β , referred to as roll and yaw, respectively. These, together with the true anomaly θ , define the attitude of the satellite's principal axes x,y,z with respect to the inertial reference frame x',y',z' as indicated in Figure 2.1. The rotor and platform spin in the x,y,z reference with angular velocities $\dot{\alpha}$ and $\dot{\lambda}$, respectively.

From the geometry of the motion, the following relations for angular velocities are readily obtained:

$$\omega_{x,I} = \dot{\alpha} - \dot{\gamma}\sin\beta + \dot{\theta}\cos\beta\cos\gamma \quad ; \quad (2.1a)$$

$$\omega_{x,II} = \dot{\lambda} - \dot{\gamma}\sin\beta + \dot{\theta}\cos\beta\cos\gamma \quad ; \quad (2.1b)$$

$$\omega_y = \dot{\beta} - \dot{\theta}\sin\gamma \quad ; \quad (2.1c)$$

$$\omega_z = \dot{\gamma}\cos\beta + \dot{\theta}\sin\beta\sin\gamma \quad . \quad (2.1d)$$

Based on the geometry and mass distribution of the satellite it is convenient to define:

I = inertia parameter of an axisymmetric satellite

$$\begin{aligned} &= I_{xx} / I_{yy} \\ &= I_{xx} / I_{zz} \quad ; \quad \text{and} \end{aligned} \quad (2.2a)$$

J = platform inertia fraction

$$= I_{xp} / I_{xx} \quad (2.2b)$$

The direction cosines of the local vertical (\hat{j}_0) along x, y, z directions are :

$$\begin{aligned} l_x &= \sin\gamma \cos\beta \quad ; \\ l_y &= \cos\gamma \cos\alpha \quad ; \\ l_z &= \sin\gamma \sin\beta \cos\alpha + \cos\gamma \sin\alpha \quad . \end{aligned} \quad (2.3)$$

Since x, y, z are body fixed principal axes with origin at centre of mass of the satellite, the following relations hold:

$$\int_{m_s} x dm_s = \int_{m_s} y dm_s = \int_{m_s} z dm_s = 0 \quad ; \quad (2.4)$$

$$\int_{m_s} xy dm_s = \int_{m_s} yz dm_s = \int_{m_s} zx dm_s = 0 \quad ; \quad (2.5)$$

$$\int_{m_s} x^2 dm_s = \frac{1}{2} (I_{yy} + I_{zz} - I_{xx}) \quad ;$$

$$\int_{m_s} y^2 dm_s = \frac{1}{2} (I_{zz} + I_{xx} - I_{yy}) \quad ;$$

$$\int_{m_s} z^2 dm_s = \frac{1}{2} (I_{xx} + I_{yy} - I_{zz}) \quad . \quad (2.6)$$

2.2 Evaluation of the Energy Expressions

The expressions for the kinetic and potential energies needed for the Lagrangian formulation can be obtained quite readily,

$$\begin{aligned}
 T &= \text{kinetic energy of the satellite} \\
 &= \text{kinetic energy due to orbital motion} + \text{kinetic energy due to} \\
 &\quad \text{rotational motion} \\
 &= \frac{m_s}{2} (\dot{R}^2 + R^2 \dot{\theta}^2) + \frac{1}{2} [I_{xx} \omega_x^2 + I_{yy} \omega_y^2 + I_{zz} \omega_z^2] .
 \end{aligned}$$

Substituting from equations (2.1) and (2.2), the kinetic energy can be expressed as,

$$\begin{aligned}
 T = & \frac{m_s}{2} (\dot{R}^2 + R^2 \dot{\theta}^2) + \frac{I_{xx}}{2I} [I(1-J)(\dot{\alpha} - \dot{\gamma} \sin \beta \\
 & + \dot{\theta} \cos \beta \cos \gamma)^2 + JI (\dot{\lambda} - \dot{\gamma} \sin \beta + \dot{\theta} \cos \beta \\
 & \cos \gamma)^2 + (\dot{\beta} - \dot{\theta} \sin \gamma)^2 + (\dot{\gamma} \cos \beta + \\
 & \dot{\theta} \sin \beta \cos \gamma)^2] . \tag{2.7}
 \end{aligned}$$

U_g = potential energy of the satellite

$$= - \int_{m_s} \frac{\mu dm_s}{|r|} ,$$

where

$$r = (x + Rl_x) \bar{i} + (y + Rl_y) \bar{j} + (z + Rl_z) \bar{k} .$$

Using expressions (2.1) to (2.6), the potential energy to $O\left(\frac{1}{R^3}\right)$ can be shown to be,

$$U_g = \frac{\mu m s}{2} - \mu \left\{ \frac{I_{xx}}{2R^3} \left(\frac{I-1}{I} \right) \right\} (1 - 3\sin^2\gamma \cos^2\beta) . \quad (2.8)$$

2.3 Nonconservative Forces and Constants of Motion

The Rayleigh dissipation function is defined as

$$F = \frac{1}{2} K_d (\dot{\alpha} - \dot{\lambda})^2 . \quad (2.9)$$

The classical Lagrangian procedure applied to the α -degree of freedom yields,

$$\frac{d}{dt} \{ I_{xr} (\dot{\alpha} - \dot{\gamma} \sin\beta + \dot{\theta} \cos\beta \cos\gamma) \} + K_d (\dot{\alpha} - \dot{\lambda}) = N_\alpha . \quad (2.10)$$

For a dual spin satellite the rotor is spun at a constant average rate, i.e., without any spin decay. The spin energy dissipated (say through bearing losses) should be compensated by means of an energy source. The generalized force N_α achieves this through

$$N_\alpha = K_d (\dot{\alpha} - \dot{\lambda}) . \quad (2.11)$$

Integration of (2.10) then yields a constant of the motion,

$$\dot{\alpha} - \dot{\gamma} \sin\beta + \dot{\theta} \cos\beta \cos\gamma = l_\alpha . \quad (2.12)$$

This may be used to eliminate the cyclic coordinate α through the spin parameter σ defined as

$$\sigma = \frac{\dot{a}}{\dot{\beta}} \Big|_{\theta=\beta=\gamma=0} = \frac{1}{\dot{\theta}} \frac{da}{d\theta} \Big|_{\theta=0}^{-1}. \quad (2.13)$$

Note, the formulation also assumes absence of energy dissipation in other degrees of freedom.

2.4 Equations of Motion

Neglecting orbital perturbations due to librational motion^{1,2} and using the spin parameter, the Lagrangian procedure yields the governing equations of motion in the roll(γ), yaw(β) and pitch(λ) degrees of freedom. Recognizing that:

$$\frac{d}{dt} = \dot{\theta} \frac{d}{d\theta};$$

$$\frac{d^2}{dt^2} = \ddot{\theta} \frac{d}{d\theta} + \dot{\theta}^2 \frac{d^2}{d\theta^2};$$

the independent variable t can be replaced by the true anomaly θ . Finally employing the classical Keplerian relations, the equations of librational motion can be written as:

$$\begin{aligned} \gamma'' - 2\beta'(\gamma'\tan\beta - \cos\gamma) - (\beta' - \sin\gamma)\sec\beta[(1-J) \\ I(\sigma+1)\left\{\frac{(1+e)}{(1+e\cos\theta)}\right\}^2 + JI(\lambda'\gamma' \\ \sin\beta + \cos\beta\cos\gamma) + \left\{\frac{3(I-1)}{(1+e\cos\theta)}\right. \\ \left. - 1\right\}\sin\gamma\cos\gamma - \left\{\frac{2e\sin\theta}{(1+e\cos\theta)}\right\} \\ (\gamma' + \cos\gamma\tan\beta) = Q_\gamma; \end{aligned} \quad (2.14a)$$

$$\begin{aligned}
\beta'' - \gamma' \cos \gamma - \{2e \sin \theta / (1 + e \cos \theta)\} (\beta' - \sin \gamma) \\
+ (\gamma' \cos \beta + \cos \gamma \sin \beta) [(1+J)I(\sigma+1) \\
\{(1+e)/(1+e \cos \theta)\}^2 + JI(\lambda' - \gamma' \sin \beta + \\
\cos \beta \cos \gamma) + (\gamma' \sin \beta - \cos \beta \cos \gamma)] - \\
\{3(I-1)/(1+e \cos \theta)\} \sin^2 \gamma \sin \beta \cos \beta = Q_\beta ; \quad (2.14b)
\end{aligned}$$

$$\begin{aligned}
\lambda'' - \gamma'' \sin \beta \{2e \sin \theta / (1 + e \cos \theta)\} (\lambda' - \gamma' \sin \beta \\
+ \cos \beta \cos \gamma) - \beta' \gamma' \cos \beta - \gamma' \cos \beta \sin \gamma - \\
\beta' \cos \gamma \sin \beta + (K/JI) \{(1+e)^{3/2} / (1+e \cos \theta)^2\} \\
[\lambda' - \gamma' \sin \beta + \cos \beta \cos \gamma - (\sigma + 1) \\
\{(1+e)/(1+e \cos \theta)\}^2] = Q_\lambda ; \quad (2.14c)
\end{aligned}$$

where Q_i ($i = \gamma, \beta, \lambda$) represent the normalized generalized forces due to solar radiation pressure which are related to the generalized forces N_i ($i = \gamma, \beta, \lambda$) by:

$$Q_\gamma = N_\gamma \frac{R^3 (1+e)^3}{I_{zz} \mu (1+e \cos \theta)^4} ;$$

$$Q_\beta = N_\beta \frac{R^3 (1+e)^3}{I_{yy} \mu (1+e \cos \theta)^4} ;$$

$$Q_\lambda = N_\lambda \frac{R^3}{I_{xx} \mu} \frac{(1+e)^3}{(1+e \cos \theta)^4}. \quad (2.15)$$

This highly nonlinear, nonautonomous and coupled system is not amenable to any closed form solution. The equations were solved numerically using an Adams-type predictor-corrector method available in the University's computer centre library^{20,21}.

3. CONTROLLER CONFIGURATION AND GENERALIZED FORCES

3.1 Description of the Controller

The normalized generalized forces (Q_i) on the right hand side of the equations of librational motion are provided by moments generated on the controller plates by the solar radiation pressure. The controller's geometry and orientation are identified with respect to the satellite's principal axis x,y,z as shown in Figure 3.1. Each of the controller plates is capable of three independent rotations α_1 , α_2 and δ . Thus the two plates taken together constitute a six degree of freedom system. When all of the six plate rotations are zero, the plate normal \hat{n} is aligned in the $-z$ direction. The plates are reflective and hence effective on both sides. The movement of the controller plates is constrained so as not to intercept the satellite body. This translates to a mathematical constraint described later in Chapter 4.

3.2 Evaluation of the Solar Radiation Pressure Force

Consider a plate element of area dA (Figure 3.2) with reflectivity ρ , transmissivity τ , and the sunlight incident at angle ξ . The resultant force due to the solar radiation pressure p_0 is given by

$$d\bar{F} = -p_0 dA |\cos \xi| \{ (1-\tau)\hat{u} + \rho\hat{s} \}. \quad (3.1)$$

With plates made of a highly reflective material, one can neglect the absorption, that is,

$$1-\tau \approx \rho,$$

giving

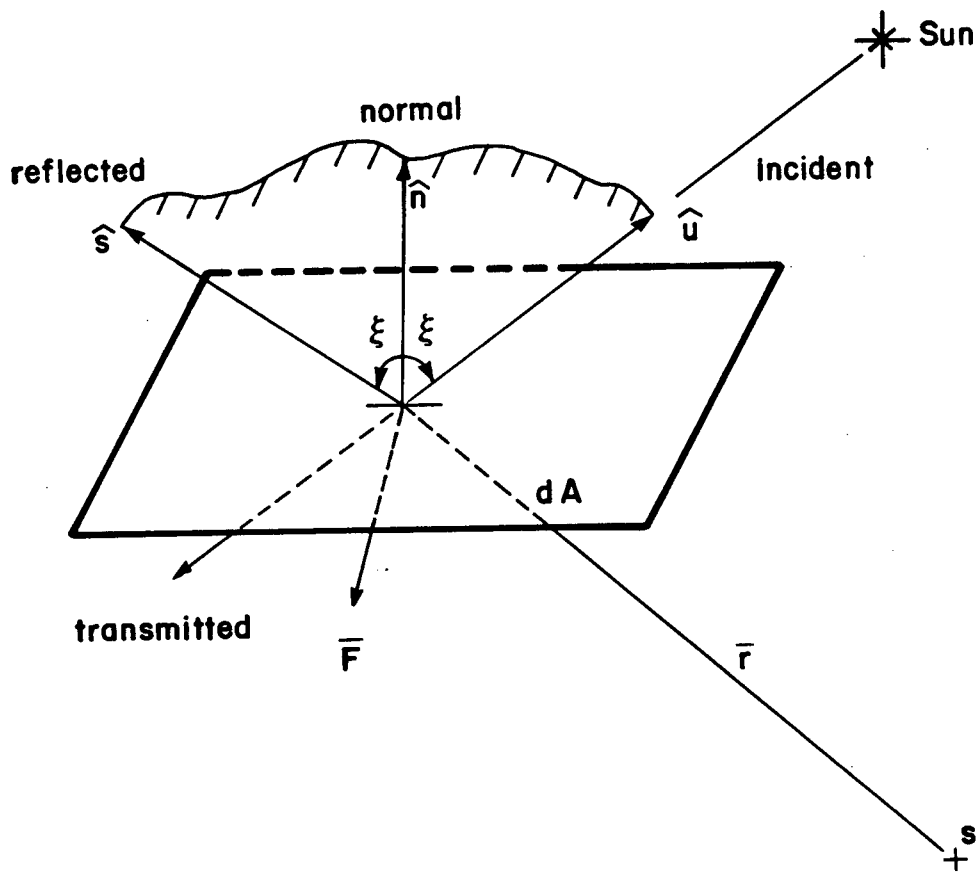


Figure 3.2 Orientation of a plate element and solar pressure force components.

$$d\bar{F} = 2\rho p_0 dA |\cos\xi| \cos\xi \hat{n}. \quad (3.2)$$

Integration over the entire plate area gives the resultant force acting at the centre of pressure of the plate,

$$\bar{F} = 2\rho p_0 A |\cos\xi| \cos\xi \hat{n}. \quad (3.3)$$

3.3 Determination of the Controller Plate Orientation

The general orientation of the controller arm and the plate determine the moment arm and angle of incidence ξ , respectively. The controller plate surface normal \hat{n} , defines the orientation of the plate after three rotations.

Initially the plate normal is directed along $-z_1$,

$$\hat{n}_1 = -\bar{k} = \begin{Bmatrix} x_1 \\ y_1 \\ z_1 \end{Bmatrix} = \begin{Bmatrix} 0 \\ 0 \\ -1 \end{Bmatrix}. \quad (3.4)$$

For rotations through δ about y_1 , α_2 about z_2 and α_1 about x_3 , the transformations between intermediate coordinates can be written as:

$$\begin{Bmatrix} x_2 \\ y_2 \\ z_2 \end{Bmatrix} = \begin{bmatrix} \cos\delta & 0 & \sin\delta \\ 0 & 1 & 0 \\ -\sin\delta & 0 & \cos\delta \end{bmatrix} \begin{Bmatrix} x_1 \\ y_1 \\ z_1 \end{Bmatrix}; \quad (3.5)$$

$$\begin{pmatrix} x_3 \\ y_3 \\ z_3 \end{pmatrix} = \begin{bmatrix} \cos a_2 & \sin a_2 & 0 \\ -\sin a_2 & \cos a_2 & 0 \\ 0 & 0 & 1 \end{bmatrix} \begin{pmatrix} x_2 \\ y_2 \\ z_2 \end{pmatrix} ; \quad (3.6)$$

$$\begin{pmatrix} x \\ y \\ z \end{pmatrix} = \begin{bmatrix} 1 & 0 & 0 \\ 0 & \cos a_1 & -\sin a_1 \\ 0 & \sin a_1 & \cos a_1 \end{bmatrix} \begin{pmatrix} x_3 \\ y_3 \\ z_3 \end{pmatrix} ; \quad (3.7)$$

giving

$$\hat{n} = \begin{pmatrix} -\cos a_2 \sin \delta \\ \cos a_1 \sin a_2 \sin \delta + \sin a_1 \cos \delta \\ \sin a_1 \sin a_2 \sin \delta + \cos a_1 \cos \delta \end{pmatrix} . \quad (3.8)$$

Thus,

$$\begin{aligned} \cos \xi = \hat{n} \cdot \hat{u} = & -u_1 (\cos a_2 \sin \delta) + u_j (\cos a_1 \sin a_2 \sin \delta + \\ & \sin a_1 \cos \delta + u_k (\sin a_1 \sin a_2 \sin \delta - \\ & \cos a_1 \cos \delta) , \end{aligned} \quad (3.9)$$

where \hat{u} = unit Sun position vector.

3.4 Position of the Centre of Pressure in Principal Coordinates

The evaluation of \bar{r} , the position vector of the centre of pressure, proceeds in a manner similar to that of \hat{n} except that there is no δ rotation,

$$\bar{r} = \bar{r}_O \pm h\bar{i}, \quad (3.10)$$

where the positive and negative signs refer to the upper and lower arms, respectively. \bar{r}_O is measured from the controller arm hinge point while h is measured from S . Initially, the centre of pressure is located at a distance ϵ in positive y_2 direction,

$$\bar{r}_O = \epsilon \bar{j}_2 .$$

On applying rotations a_2 followed by a_1 , the vector \bar{r}_O in the principal coordinates is given by,

$$\bar{r}_O = \epsilon \begin{pmatrix} \sin a_2 \\ \cos a_1 \cos a_2 \\ \sin a_1 \cos a_2 \end{pmatrix} , \quad (3.11)$$

i.e.,

$$\bar{r} = \epsilon \begin{pmatrix} \sin a_2 \pm h/\epsilon \\ \cos a_1 \cos a_2 \\ \sin a_1 \cos a_2 \end{pmatrix} . \quad (3.12)$$

3.5 Evaluation of the Controller Plate Moments and Generalized Forces

The moment produced by each controller plate is given by,

$$\mathbf{N} = \int_A \bar{\mathbf{r}} \times d\bar{\mathbf{F}} = \bar{\mathbf{r}} \times \bar{\mathbf{F}},$$

where $\bar{\mathbf{F}}$ is substituted from equation (3.3) to yield

$$\mathbf{N} = 2\rho p_0 A |\cos\xi| \cos\xi \bar{\mathbf{r}} \times \hat{\mathbf{n}}. \quad (3.13)$$

Using equations (3.8) and (3.12), $\bar{\mathbf{r}} \times \hat{\mathbf{n}}$ can be evaluated giving the control moment components as:

$$N_x = 2\epsilon\rho p_0 A |\cos\xi| \cos\xi \cos a_2 \cos\delta;$$

$$N_y = -2\epsilon\rho p_0 A |\cos\xi| \cos\xi [\pm(h/\epsilon)(\cos a_1 \cos\delta - \sin a_1 \sin a_2 \sin\delta) + \cos a_1 \sin a_2 \cos\delta - \sin a_1 \sin\delta];$$

$$N_z = -2\epsilon\rho p_0 A |\cos\xi| \cos\xi [\pm(h/\epsilon) + \sin a_2 (\sin a_1 \cos\delta + \cos a_1 \sin a_2 \sin\delta) + \cos a_1 \cos^2 a_2 \sin\delta]. \quad (3.14)$$

The resultant moment consists of contributions from the upper and lower plates,

$$\mathbf{N} = \mathbf{N}_U + \mathbf{N}_I . \quad (3.15)$$

The generalized forces can now be obtained quite readily. Equations (3.14) give the moments along the orthogonal directions x,y,z (Figure 2.1). The generalized moments $N_\gamma, N_\beta, N_\lambda$ can be related to them through projections along principal coordinate directions after application of the corresponding Eulerian rotations γ, β, λ .

N_γ is applied first along z_0 axis (γ axis) resulting in rotation γ with the first moment projections,

$$\begin{Bmatrix} N_{x_1} \\ N_{y_1} \\ N_{z_1} \end{Bmatrix} = \begin{bmatrix} \cos\gamma & \sin\gamma & 0 \\ -\sin\gamma & \cos\gamma & 0 \\ 0 & 0 & 1 \end{bmatrix} \begin{Bmatrix} 0 \\ 0 \\ N_\gamma \end{Bmatrix} = \begin{Bmatrix} 0 \\ 0 \\ N_\gamma \end{Bmatrix} .$$

N_β is applied next along the y_1 axis (β axis) causing rotation β with the projections,

$$\begin{Bmatrix} N_{x_2} \\ N_{y_2} \\ N_{z_2} \end{Bmatrix} = \begin{bmatrix} \cos\beta & 0 & -\sin\beta \\ 0 & 1 & 0 \\ \sin\beta & 0 & \cos\beta \end{bmatrix} \begin{Bmatrix} 0 \\ N_\beta \\ N_\gamma \end{Bmatrix} = \begin{Bmatrix} -\sin\beta N_\gamma \\ N_\beta \\ \cos\beta N_\gamma \end{Bmatrix} .$$

Finally N_λ is applied along x_2 axis leading to rotation λ . However, the principal body coordinates do not rotate with λ , so N_λ is simply added to the N_{x_2} component to give the final moment vector in the principal body coordinates,

$$\begin{Bmatrix} N_x \\ N_y \\ N_z \end{Bmatrix} = \begin{bmatrix} 1 & 0 & -\sin\beta \\ 0 & 1 & 0 \\ 0 & 0 & \cos\beta \end{bmatrix} \begin{Bmatrix} N_\lambda \\ N_\beta \\ N_\gamma \end{Bmatrix}. \quad (3.16)$$

The generalized moments can now be determined from the known moments N_x, N_y, N_z by inverting the transformation (equation 3.16),

$$\begin{Bmatrix} N_\lambda \\ N_\beta \\ N_\gamma \end{Bmatrix} = \begin{bmatrix} 1 & 0 & \tan\beta \\ 0 & 1 & 0 \\ 0 & 0 & \sec\beta \end{bmatrix} \begin{Bmatrix} N_x \\ N_y \\ N_z \end{Bmatrix}. \quad (3.17)$$

Applying equations (2.15a), (2.15b) and (2.15c) one obtains the normalized generalized forces,

$$\begin{Bmatrix} Q_\lambda \\ Q_\beta \\ Q_\gamma \end{Bmatrix} = \Pi \begin{bmatrix} 1 & 0 & \tan\beta \\ 0 & 1 & 0 \\ 0 & 0 & \sec\beta \end{bmatrix} \begin{Bmatrix} N_x \\ N_y \\ N_z \end{Bmatrix}, \quad (3.18)$$

$$\text{where } \Pi = \frac{R^3 (1+e)^3}{I_{xx} \mu (1+e \cos\theta)^4}.$$

The constants of equation (3.18) can be combined with those common to equations (3.14) giving the dimensionless *controller dynamics parameter*,

$$C = \frac{2\epsilon\rho p_0 R^3 A}{I_{xx} \mu}. \quad (3.19)$$

Thus the normalized generalized moment vector has the form,

$$\begin{pmatrix} Q_\lambda \\ Q_\beta \\ Q_\gamma \end{pmatrix} = CE(\theta) |\cos\xi| \cos\xi \begin{bmatrix} 1 & 0 & \tan\beta \\ 0 & 1 & 0 \\ 0 & 0 & \sec\beta \end{bmatrix} \begin{pmatrix} N_{px} \\ N_{py} \\ N_{pz} \end{pmatrix}, \quad (3.18)$$

where:

$$N_{px} = \cos a_2 \cos \delta ;$$

$$N_{py} = - [\pm(h/\epsilon)(\cos a_1 \cos \delta \sin a_1 \sin a_2 \sin \delta) \\ + \cos a_1 \sin a_2 \cos \delta - \sin a_1 \sin \delta] ;$$

$$N_{pz} = - [\pm(h/\epsilon) + \sin a_2) (\sin a_1 \cos \delta + \\ \cos a_1 \sin a_2 \sin \delta) + \cos a_1 \cos^2 a_2 \sin \delta];$$

$$E(\theta) = \frac{(1+e)^3}{(1+e \cos \theta)^4} .$$

The highly transcendental character of the generalized forces does not permit closed form determination of the plate orientation for a desired moment Q . Note also that the problem is underspecified, i.e., there are three equations and six unknowns.

4. CONTROL PHILOSOPHY AND OPTIMIZATION OF GENERALIZED FORCES

4.1 Introduction

As outlined earlier, the generalized forces are quite complex, necessitating the development of a control philosophy particularly suited to the physics of the controller. The solar radiation pressure force, though dominant (relative to other environmental forces), provides only a weak control moment. On the positive side, the well developed theory of gyroscopes can be used to advantage because a dual spin satellite in space behaves exactly as a disturbed gyroscope. It may be noted that the theory can be easily extended to nondual spin spacecraft by simply setting the spin parameter σ to zero (Chapter 2, equation 2.13).

Thus the following guidelines emerged in the design of the control strategy:

- (a) utilize the theory of gyroscopes to judiciously choose the direction in which the optimal control moment \mathbf{N} should be applied, independent of its magnitude, to stabilize the spacecraft;
- (b) maximize the weak solar radiation pressure moment along the direction.

The principles imply that application of a nonlinear optimization technique, such as the projected gradient method, would be the best means of solving the controller equations. Furthermore, since the controller equations are underspecified, (six unknowns with three equations) we would require at least three constraint equations. This translates into the following optimization problem:

Minimize the cost function F , subject to the constraint given by vector $\mathbf{g}=0$.

where:

$$F = -\mathbf{N}_d \cdot \mathbf{N}; \quad (4.1a)$$

and

$$\mathbf{g} = \begin{pmatrix} g_1 \\ g_2 \\ g_3 \end{pmatrix} = 0. \quad (4.1b)$$

Functions g_1 , g_2 and g_3 are described in section 4.2. The cost function implies that we wish to maximize the component of the control moment \mathbf{N} along the desired moment direction \mathbf{N}_d subject to the constraints represented by equation (4.1b).

4.2 Constraints of the Problem

Directional Constraint

The directional constraint ensures that \mathbf{N} acts along \mathbf{N}_d and has the form,

$$g_1 = \left[2 \left\{ 1 - \frac{\mathbf{N} \cdot \mathbf{N}_d}{|\mathbf{N}| |\mathbf{N}_d|} \right\} \right]^{1/2}. \quad (4.2a)$$

This function closely approximates the angle (in radians) between \mathbf{N} and \mathbf{N}_d when they are nearly aligned. The function, therefore, has the following desirable properties:

- (i) its solution is unique, that is, equation (4.2a) is satisfied only when \mathbf{N} and \mathbf{N}_d are exactly in the same direction;
- (ii) it permits specification of the maximum acceptable misalignment between \mathbf{N} and \mathbf{N}_d to act as the stopping condition for the method used to solve equation (4.2a).

Mechanical Constraints

The mechanical constraints ensure that the controller arms and plates do not move in a way as to interfere with any part of the satellite. This requires that $a_2^u > 0$ and $a_2^l < 0$ as shown in Figure 3.1:

$$g_2 = \begin{cases} 0 & , & a_2^u \geq 0 & , \\ a_2^u & , & a_2^u < 0 & ; \end{cases} \quad (4.2b)$$

$$g_3 = \begin{cases} 0 & , & a_2^l \leq 0 & , \\ a_2^l & , & a_2^l > 0 & . \end{cases} \quad (4.2c)$$

Since the gradient of the vector g does not exist on the constraint surface (Appendix A), the nonlinear constrained optimization technique mentioned earlier cannot be used. Instead, a similar two step approach is employed that economically permitted near second-order convergence to the constrained minimum of F .

The first step attempts to achieve the constraint surface ($g=0$) using the *second-order Newton method*. The second step utilizes a combination of two unconstrained optimization techniques, *steepest descent method* and the *Fletcher-Reeves conjugate gradient method*,²² to move one increment towards the unconstrained minimum of F . This corresponds to one step of the steepest descent method or one cycle of the Fletcher-Reeves method. The above restriction prevents the system from drifting away too far from the constraint surface in the pursuit of the minimum of F as the increment, in general, is not along the constraint surface.

Step one is then reactivated to reach the constraint surface again. Thus, by repeated application of step one and step two in sequence, the constrained minimum of F is obtained.

4.3 The Constraint Surface

The second order Newton method is utilized to achieve the constraint surface. The foundation of this technique is the Taylor series approximation upto first order variation,

$$g(x_{k+1}) \approx g(x_k) + g_x \Delta x = 0,$$

Where x is a vector comprised of the six controller plate rotations and g_x is the gradient or the Jacobian matrix of g . $g(x_k)$ is the current value of the constraint vector g . The method leads to the next smaller constraint vector, $g(x_{k+1})$, in steps of size

$$\Delta x = -g_x' [g_x g_x']^{-1} g(x_k), \quad (4.3)$$

resulting in a plate rotation update of

$$x_{k+1} = x_k + \Delta x. \quad (4.4)$$

The iteration stops when $|g(x_k)|$ becomes less than a preset error tolerance, t , expressed in radians,

$$|g(x_k)| < t \approx 0.$$

One of the difficulties of this method lies in the inversion $[\mathbf{g}_x \mathbf{g}_x']^{-1}$ in equation (4.3). When the mechanical constraints of equations (4.2b) and (4.2c) are satisfied, the matrix reduces to a simple constant whose inversion produces no problem when non-zero. However, when the mechanical constraints are not satisfied, the matrix could be singular. This problem was overcome by using a random number generator to produce a series of uniformly distributed random numbers of extent $\pm t$. When added to the plate rotations, they act as a disturbance and perturb the system off the singular point. Fortunately, this problem was never encountered.

A complication may arise when one of the mechanical constraints (g_2 or g_3) is zero implying that the gradient at the constraint is also zero. This results in a zero element row and column in the $\mathbf{g}_x \mathbf{g}_x'$ matrix, making it singular. The problem, however, can be overcome by noting that a constraint which is satisfied represents the one that is no longer active. It can, therefore, be temporarily removed from consideration by reduction of the matrix (by removal of zero row and column) prior to inversion. After inversion the zero row and column are once more restored and the computational process continues.

4.4 Unconstrained Minimization

Once the constraint surface is obtained, a combination of two techniques, as mentioned before, is implemented to minimize F . Initially, the steepest descent gradient method rapidly guided the system to a minimum. When close to the solution, the Fletcher-Reeves conjugate gradient method was used for finer second order convergence. The criterion used for determining closeness to the solution was

$$|\Delta x_i| \leq 20t,$$

where $|\Delta x_i|$ represents the largest plate rotational increment in a given step. The above approach was preferred to second-order Newton-Raphson method because the latter would involve inversion of the cost function's Hessian matrix. Obviously, this is computationally costly. More importantly, since F can readily be shown to have a maximum as well as a minimum, the Hessian matrix of F is not always positive definite. Therefore, a true second-order method could inadvertently drive the system to the maximum. In comparison, the steepest descent gradient method is easy to implement and is guaranteed to converge to a minimum. However, near the minimum the convergence rate of the gradient method can become quite slow. For this reason the Fletcher-Reeves method is invoked in this region. The Fletcher-Reeves method only requires the computation of the gradient of the cost function which is easier and far less time consuming.

The steepest descent gradient method determines the current search direction by utilizing the gradient of the cost function, F , denoted by F_x .

$$S_k = -\frac{F_x}{|F_x|} \quad (4.5)$$

The next lowest value of F is located at a distance D_k from the current point in the direction S_k . The new plate rotations are then updated from the previous values

$$x_{k+1} = x_k + D_k S_k \quad (4.6)$$

D_k is evaluated through a linear search discussed later. This process continues until the change in plate rotations between successive optimal points on the constraint surface becomes less than 20t. At this point the Fletcher-Reeves conjugate gradient method takes over. This is a multistep cycle requiring as many iterations as there are dimensions to the problem (six in the present case).

The first step is a steepest descent gradient search exactly the same as in equations (4.5) and (4.6) above. The subsequent five steps involve the current cost function gradient $F_{x,k}$ and previous cost function gradient $F_{x,k-1}$. The new search direction is given by

$$S_k = \frac{d_k}{|d_k|}, \quad (4.7)$$

$$\text{where } d_k = -F_{x,k} + \frac{|F_{x,k}|^2}{|F_{x,k-1}|^2} d_{k-1}. \quad (4.8)$$

Initially $d_0 = F_{x,0}$, i.e., the gradient of the cost function in the first step. x_k is updated as in equation (4.6). Each cycle produces a second order convergence step just as the Newton-Raphson method does but is less time consuming as only the gradient of the cost function has to be computed in each interval.

A linear search in the direction of S_k is employed by both the techniques, namely, the steepest descent gradient method and the Fletcher-Reeves method. This search is conducted using the secant method out to a maximum distance of ten degrees from the current point x_k . The secant search seeks to find the zero of the directional derivative of F along S_k . The secant method updates D_k through the recursive relation,

$$D_{k+1} = D_{k-1} - (D_k - D_{k-1}) \frac{F_D(D_{k-1})}{F_D(D_k) - F_D(D_{k-1})}, \quad (4.9)$$

where F_D is the directional derivative of F . Initially D_k is set within the ten degree bound, but it is reduced if D_{k+1} falls outside the zero to ten degree region. The iterations stop when D_k is less than t .

4.5 Some Further Remarks

The algorithm was found to be quite efficient and robust. Irrespective of the starting point, it was able to drive the system to the constraint surface and then attain the objective function minimum. Selection of a starting point for the constrained optimization involved two choices. On initiation of the satellite control, or when the current moment direction differed from the previous moment direction by more than thirty degrees, the controller plates were assigned zero-moment position facing the sun flat-on. Since at this orientation each plate individually is producing the maximum force, it was felt that fewer iterations may be needed to achieve the optimal combined directed moment. When the previous current moment directions differed by less than thirty degrees, the corresponding plate rotations are used as the starting guess, thereby possibly reducing the number of iterations required.

Occasionally some difficulty was encountered when the cost-function F had a non-negative value on completion of a constrained optimization phase. This implied that \mathbf{N} was directed opposite to \mathbf{N}_d . However, this phenomenon was rare and was never observed to occur consecutively in two control action intervals. When h/ϵ was specified greater than unity, the solution became more tedious and error prone, though the failure rate remained less than 0.5% and was usually zero for $h/\epsilon = 1$. It may be noted that these failures may also be due to the bounds placed on the iteration counts in the method to prevent computing costs from becoming prohibitive. During such failures the satellite was simply coasted without applied moment for one interval and then the control action was resumed.

Yet another problem was encountered during implementation of the constrained optimization algorithm, however this was attended through a minor modification of the controller moment gradient. From equation (3.14) we see that the term $|\cos \xi|$ multiplies all the three components of the controller moment \mathbf{N} . If

plates are edge on to the sun, the $|\cos\xi|$ term becomes zero resulting in the moments and their gradients becoming zero. Thus a saddle point is obtained in the optimization equations. Since the optimization algorithm requires a non-zero gradient to proceed, it will stop at such a point. The problem was avoided by forcing $|\cos\xi| \geq 0.02$ in the calculation of the moment Jacobian matrix. This preserved a gradient of $|\cos\xi|$ at the saddle point permitting the algorithm to proceed.

4.6 Nature of the Controller Moments and Practical Feasibility of the Controller

The use of a magnitude independent strategy can be justified by consideration of the nature of the controller moments that are available. If the maximum moment \mathbf{N} available in all directions about the satellite for various solar positions and controller offset ratios h/ϵ is plotted, one obtains a series of surfaces. It may be noted that these surfaces may be compiled with relative ease owing to the symmetric nature of the problem. Firstly, because of overall symmetry of the entire system about the x -axis, the results of all solar positions can be obtained by moving the solar vector \mathbf{u} in any fixed plane normal to the y - z plane. The elevation of \mathbf{u} can now be specified by a single angle Ω . Further symmetries, discussed in Appendix-B, imply that the calculation of the optimal moments for one-half of a hemisphere about the satellite is sufficient to generate the remaining moment directions through a series of reflections and rotations, thus saving a great deal of computer effort. Figures (4.1a) to (4.1d) show the surfaces obtained for $h/\epsilon=1$ for four different solar elevation angles with \mathbf{u} in the x - y plane. The unseen part of each surface is obtained by reflecting the observed points about the z axis. Inverting the figures would show the result for negative Ω .

Three features become immediately apparent from these surfaces:

- (i) they are convoluted, i.e., there can be abrupt changes in minima;

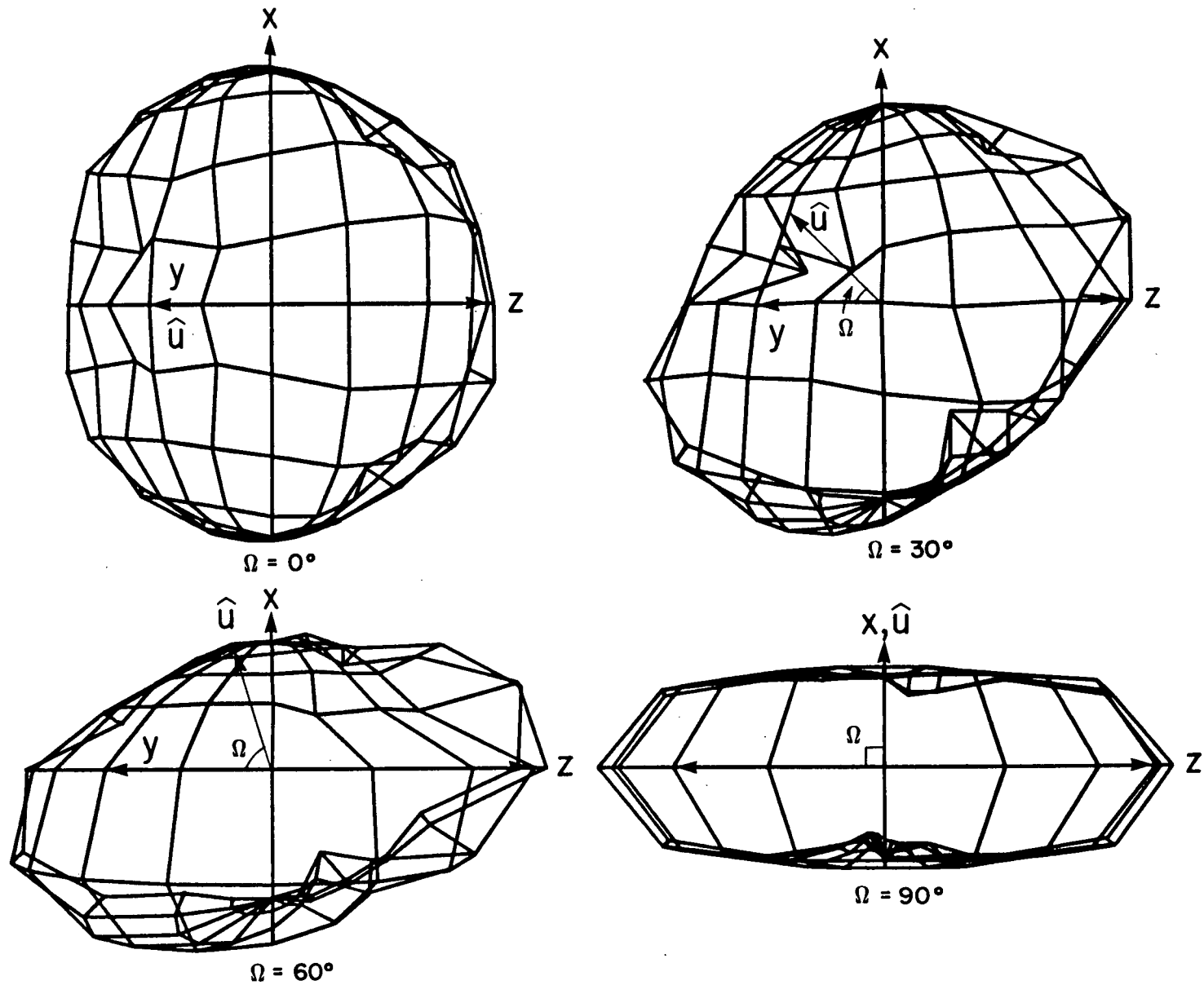


Figure 4.1 Maximum controller moment surfaces under varying solar elevation angles.

- (ii) they become increasingly flattened for increasing Ω ;
- (iii) as h/ϵ becomes larger, both the above features are increasingly emphasized.

These results indicate that for an arbitrary satellite orientation (i.e., arbitrary Ω), any specific moment cannot be guaranteed in all directions. However, some moment seems to be available in any direction. Thus a magnitude independent strategy would prove successful.

The physical implementation of the moment optimization also has to be justified with respect to a real satellite. During simulations, it was observed that the proposed optimization procedure and associated control strategy (presented in the next chapter) not only operated satisfactorily but also quite rapidly. As an example, stabilization of a disturbed satellite during one hundredth of an orbit, took about 87 seconds on an Amdahl 470-V8 computer. Hence the controller would have sufficient time per step to achieve the control action in actual orbit. The fact that a large mainframe processor was employed does not detract from the feasibility of achieving similar performance with a dedicated processor on board the spacecraft.

However, it is recognized that the complete optimization procedure as outlined here would involve a great deal of computational resources. The moment surfaces of Figure 4.1 provide an avenue for streamlining the optimization procedure considerably and for improving its reliability. The search time of any optimization algorithm and the reliability of its convergence to a global minimum depend strongly on the starting point chosen. Figures (4.1a) to (4.1d) indicate the moment directions for a given solar elevation angle for which the plate rotations are known. A series of such surfaces could be rigorously evaluated to an arbitrary angular resolution during satellite development on Earth, and then stored as 'read only' memory in the satellite control computer. Such storage would be rendered more economical by utilizing the symmetries described in Appendix B thus involving grid

points only over one-quarter of a sphere. Given such a data base, convergence to an optimal moment for a given direction \mathbf{N}_0 would entail first a choice of the closest direction and solar elevation for which there is a stored solution, and then use of that solution as the starting point for the constrained optimization algorithm. Such an approach would involve far fewer iterations to converge to the optimal plate rotations.

5. CONTROL STRATEGY

5.1 Nature and Objective of the Control Strategy

The objective of the control strategy is to determine the desired moment direction \mathbf{N}_d . This is achieved through a knowledge of the spacecraft's dynamical relations together with an application of the theory of gyroscope. Once the appropriate moment direction has been identified, the optimization procedure outlined earlier specifies the controller plate angles to achieve maximum moment \mathbf{N} in that direction subject to the constraints.

It is necessary to base the strategy on readily measurable parameters concerning the satellite's immediate dynamics. The parameters used are:

- (i) satellite's position relative to the fixed stars (Ω, ω) ;
- (ii) angular velocity of the satellite ($\dot{\gamma}, \dot{\beta}, \dot{\lambda}$) ;
- (iii) the Sun's position relative to the satellite (i, ϕ) ;
- (iv) Earth's position relative to the satellite (R, θ, e) .

Furthermore, the strategy should be such that it depends only on the applied moment's direction to achieve a desired result. A quantity is therefore sought whose direction as well as magnitude changes in proportion to the applied moment. The satellite's angular momentum, \mathbf{L} , represents such a quantity. The applied moment \mathbf{N} is related to the angular momentum \mathbf{L} , through the classical relation

$$\frac{d\mathbf{L}}{dt} = \mathbf{N} ,$$

for a reference coordinate system that is either inertial or fixed to the body at its centre of mass. The value of \mathbf{L} can be readily calculated from the satellite's angular velocity (roll, yaw and pitch rates) as:

$$\begin{aligned}
 L_x &= \omega_x I_{xx} + L_a \\
 &= (\dot{\lambda} - \dot{\gamma} \sin \beta + \dot{\theta} \cos \gamma \cos \beta) I_{xx} + L_a ;
 \end{aligned}
 \tag{5.1a}$$

$$\begin{aligned}
 L_y &= \omega_y I_{yy} \\
 &= (\dot{\beta} - \dot{\theta} \sin \gamma) I_{yy} ;
 \end{aligned}
 \tag{5.1b}$$

$$\begin{aligned}
 L_z &= \omega_z I_{zz} \\
 &= (\dot{\gamma} \cos \beta + \dot{\theta} \cos \gamma \sin \beta) I_{zz} .
 \end{aligned}
 \tag{5.1c}$$

Note, the angular momentum contribution of the rotor, L_a , has been accounted for.

When Euler's dynamical equations are applied to an axisymmetric body, it can be shown that the axis of symmetry precesses about L , the angular momentum vector, counterclockwise at a rate,

$$\dot{\psi} = (\omega_x^2 + \omega_y^2)^{1/2} \sin \theta_s .
 \tag{5.2}$$

The precession progresses as long as the spin and precession velocity vectors along I_s and L , respectively, are misaligned as shown in Figure 5.1. I_s is the unit vector along the axis of symmetry. This unstable situation can be remedied by promoting realignment of these vectors ($\psi \rightarrow 0$ as $\theta_s \rightarrow 0$). Ideally this aligned orientation is a fixed direction in space for all positions in the orbit, i.e., normal to the orbital plane. Furthermore, the equilibrium configuration for a spinning satellite is with the spin axis normal to the orbital plane. This direction is referred to as the reference momentum orientation L_R . In the absence of any applied moment, L_R

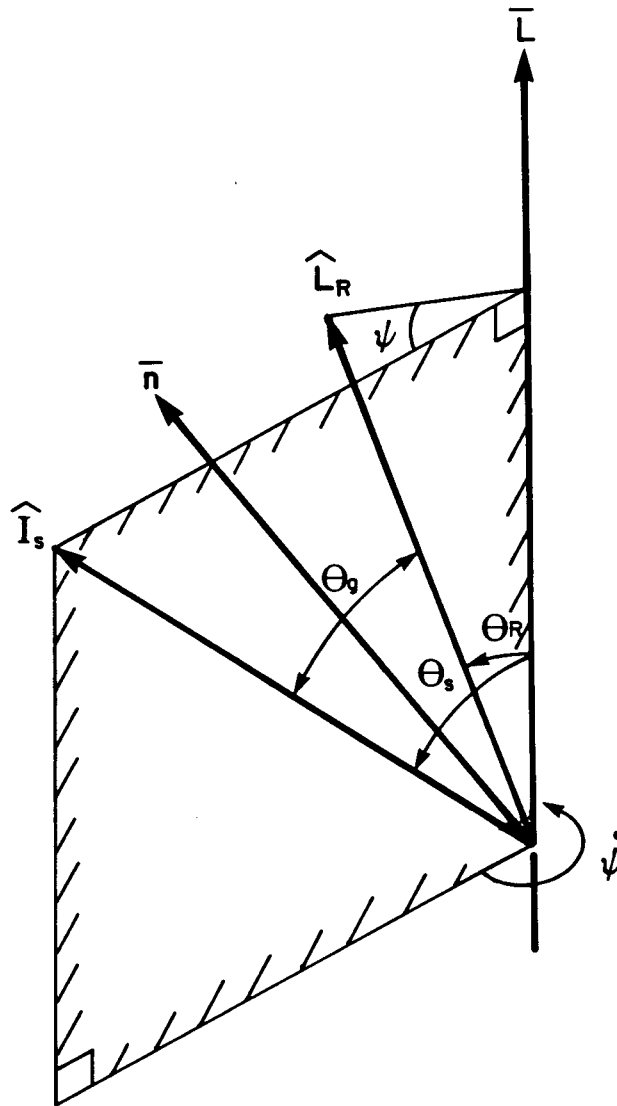


Figure 5.1

Relative geometry of the axis of symmetry, the angular momentum vector and the reference momentum vector.

maintains a fixed angle θ_R with respect to L . The vector L_R is specified by two more modified Eulerian angles (γ_f and β_f) representing the orientation of the spin axis with respect to the orbital frame. Thus, applying transformations corresponding to these rotations as indicated in Chapter 3, components of the reference momentum vector along principal coordinate directions are given by:

$$\begin{aligned} L_{Rx} &= \cos\beta [\cos\gamma \cos\gamma_f \cos\beta_f + \sin\gamma \sin\gamma_f \cos\beta_f] \\ &+ \sin\beta \sin\beta_f ; \end{aligned} \quad (5.3a)$$

$$L_{Ry} = \cos\gamma \sin\gamma_f \cos\beta_f - \sin\gamma \cos\gamma_f \cos\beta_f ; \quad (5.3b)$$

$$\begin{aligned} L_{Rz} &= \sin\beta [\cos\gamma \cos\gamma_f \cos\beta_f + \sin\gamma \sin\gamma_f \cos\beta_f] \\ &- \cos\beta \sin\beta_f . \end{aligned} \quad (5.3c)$$

The three principal angles θ_s , θ_R and θ_g are illustrated in Figure 5.1. They can be readily expressed in terms of the associated vector orientations as:

$$\theta_s = \arccos \left[\frac{I_s \cdot L}{|L|} \right] ; \quad (5.4a)$$

$$\theta_R = \arccos \left[\frac{L_R \cdot L}{|L|} \right] ; \quad (5.4b)$$

$$\theta_g = \arccos \left[\frac{I_s \cdot L_R}{|L|} \right] . \quad (5.4c)$$

Note ψ , taken to be always positive, is defined as the angle between the L_R - L and I_s - L planes.

The \mathbf{L} , \mathbf{L}_R and \mathbf{I}_S vectors form the basis of the control strategy. The controller's efforts are directed towards bringing \mathbf{L} and \mathbf{I}_S in alignment with \mathbf{L}_R which implies achievement of roll–yaw control. Final pitch control is effected through a simple time–optimal bang–bang strategy where \mathbf{N} is directed along \mathbf{I}_S .

The above mentioned vector alignment strategy is performed in several stages. The approach permits precession of \mathbf{I}_S about \mathbf{L} to bring it in alignment with \mathbf{L}_R , while manipulating \mathbf{L} to finally align with both.

Figure 5.2 shows, in the form of a flow chart, some of the important steps involved in determination of the desired control moment direction \mathbf{N}_d . In the controlled mode of operation of the satellite, the strategy routine is entered and one of the two initial branches of the flow chart is followed depending on the configuration of the vectors \mathbf{L} , \mathbf{L}_R and \mathbf{I}_S in Figure 5.1. If \mathbf{L} , \mathbf{L}_R and \mathbf{I}_S are misaligned, (i.e., θ_S , θ_R and θ_G are not all zero) the algorithm to achieve their alignment (momentum alignment) is followed. When this is accomplished, the other branch corrects for the pitch misalignment. Note, a certain amount of pitch alignment is also attempted during the momentum alignment as depicted in the flow chart.

Momentum alignment is effected by simultaneously following the three parallel paths of *alignment*, *equalization* and *pitch control*, each of which generates an orthogonal moment direction. Their resultant gives the desired direction \mathbf{N}_d , which is then utilized in the optimization routine to obtain the applied moment \mathbf{N} through appropriate plate rotations. The primary objective of alignment and equalization paths is roll–yaw control. Thus the moment direction generated in these branches is always orthogonal to \mathbf{L} so that $|\mathbf{L}|$ is not affected.

Pitch, controlled by the third path, is influenced by the other two. This necessitates the final bang–bang pitch control in the other branch. It must be noted that the flow chart has been simplified considerably in order to help comprehend the essential features of the control strategy.

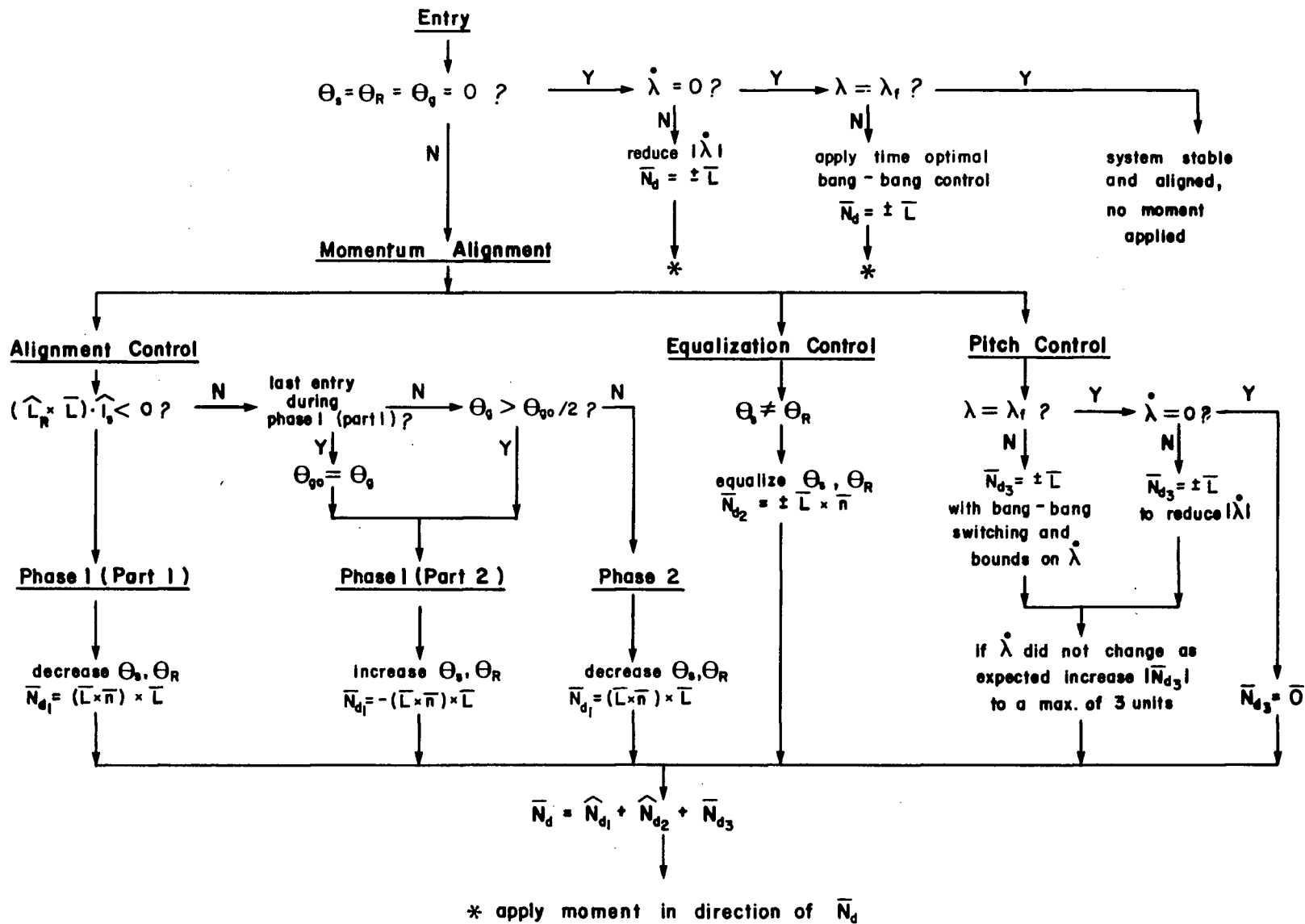


Figure 5.2

Control Strategy flow chart for equilibrium configuration as final orientation.

5.2 Alignment Control

The alignment control branch of the strategy attempts to move the angular momentum vector L in such a way as to increase the speed of convergence of I_S to L_R under the action of precession. Once this occurs, it forces convergence of the three vectors L , L_R and I_S . This assumes that equalization control has already positioned I_S suitably. The alignment control strategy consists of two phases as explained next.

Phase 1: Positioning of I_S , L_R and L for subsequent convergence

The role of Phase 1 of alignment control is to speed up the convergence of I_S to L_R and to position L suitably for convergence. This is conducted in two parts:

Part 1

Immediately following an impulsive disturbance (e.g., micrometeorite impact), L is displaced from its alignment with I_S and L_R to a position where $\theta_S = \theta_R \neq 0$. I_S and L_R remain initially aligned due to the inertia of the satellite. The effect of θ_S having a finite value causes precession ($\dot{\psi}$) to occur in accordance with equation (5.2) resulting in divergence of I_S from L_R . That is, θ_g increases. This divergence would continue until $\psi \geq 180^\circ$. Following this, convergence of the two vectors would occur with corresponding decrease in θ_g . The divergence of L_R and I_S can be stopped if L is moved to the other side of the I_S - L_R plane where the position of I_S relative to L is such that the two vectors converge and θ_g decreases.

The condition of divergence or convergence can be easily determined by the value of ψ ($\psi < 180^\circ$ or $\psi > 180^\circ$, respectively). According to the right hand rule, ψ increases in the counterclockwise sense and the condition for convergence/divergence in vector notation can be written as:

$$L_R \times L \cdot I_s \begin{cases} < 0, L_R \text{ and } I_s \text{ diverge ;} & (5.5a) \\ > 0, L_R \text{ and } I_s \text{ converge .} & (5.5b) \end{cases}$$

As soon as the satellite is subjected to a disturbance, condition (5.5a) is found to be satisfied. The direction of the applied moment, N_d , is then chosen to move L into the I_s-L_R plane with the objective of placing it, eventually, on the other side where condition (5.5b) holds.

Thus the moment is applied orthogonal to L in the direction of n , the bisector of θ_g , in order to maintain θ_s and θ_R equal throughout:

$$n = L_R + I_s ;$$

and

$$N_{d1} = (L \times n) \times L = n(L \cdot L) - L(n \cdot L) . \quad (5.6)$$

The moment is applied until L crosses the I_s-L_R plane which is detected as a fulfilment of condition (5.5b).

Part 2

When L crosses the I_s-L_R plane Part 2 of the strategy takes over. The initial value of θ_g is recorded as θ_{g0} . The precession of ψ is directed so as to cause θ_g to decrease without altering L . The period of convergence can be reduced further by simply moving L further away from the I_s-L_R plane thereby reducing the required precessional travel angle ϕ . The purpose

of Part 2, therefore, is to move L an optimal angle from the I_S-L_R plane to minimize the alignment time.

The applied moment is now directed in the same direction as in Part 1, though, the sign is altered because L is now on opposite side of the I_S-L_R plane,

$$N_{d1} = - (L \times n) \times L. \quad (5.7)$$

The dynamics is governed by this scheme until one of the following two conditions is satisfied.

$$(i) \quad \theta_g < \theta_{g0}/2 \quad (5.8)$$

This condition is based on the premise that θ_g decreases uniformly during both divergence of L in Phase 1 (Part 2) and convergence of L during Phase 2. It is quite obvious that the cut-off point cannot be exactly halfway as given in condition (5.8). This is because of several reasons:

- (a) During divergence of L the convergence of θ_g is aided, while the opposite occurs during convergence of L .
- (b) There are nonlinearities in the controller moments (e.g., due to the presence of gravity gradient torques).
- (c) ψ follows a different trajectory depending on inward or outward movement of L .

In practice, however, the actual switch point was found to be less than 2 and as low as 1.7 for large disturbances. The influence of the choice on the final result was, in general, small.

$$(ii) \quad \theta_s > 80^\circ$$

This condition sets a sufficiently safe margin such that θ_s is not permitted to increase indefinitely while awaiting condition (i) to be fulfilled. If θ_s were to exceed 90° , precession would cause divergence rather than alignment, placing the system back into Phase 1 (Part 1). In stabilization trials, this limit was seldom attained.

Phase 2: Simultaneous convergence of L , I_s and L_R

The objective in Phase 2 is to converge all the three vectors L , I_s and L_R simultaneously. Control shifts to this phase when either condition (i) or (ii) in Phase 1 (Part 2) is satisfied. The applied moment N_d is again directed normal to L in the plane $L-n$ so as to move L towards I_s and L_R . Thus the moment direction is opposite to that in Phase 1 (Part 2),

$$N_{d1} = (L \times n) \times L . \quad (5.9)$$

The moment is applied in this direction until one of the three conditions is satisfied:

(i) Overshoot

L_R and I_s come into alignment before θ_s , θ_R become zero. Further precession causes divergence of θ_g so Phase 1 (Part 1) is re-entered.

(ii) Undershoot

Here $\theta_s, \theta_R < 1.5 \theta_g$ and $\theta_g > 0$. This condition occurs if L is approaching the I_s-L_R plane while θ_g is large, making it unlikely for vector

alignment to occur on this approach. θ_g is therefore reset and Phase 1 (Part 2) is re-entered.

$$(iii) \underline{\theta_s = \theta_R = \theta_g = 0}$$

Momentum alignment, i.e., roll-yaw control is now complete. This condition is also tested in Phase 1 (Part 1). Now the second branch of the strategy for pitch control is entered.

5.3 θ_s, θ_R Equalization Control

The objective of this branch of the strategy is to maintain θ_s and θ_R equal throughout. This is necessary for the above mentioned two-phase alignment control strategy to be successful. In other words, it is necessary to ensure that L_s aligns with L_R as it passes through the L_R - L plane during precession. The tolerance allowed here is

$$|\theta_g - \theta_R| < \theta_g/10 . \quad (5.10)$$

Thus equalization becomes finer as θ_g becomes smaller. If condition (5.10) is violated, then this part of the strategy produces a moment component N_{d2} perpendicular to n - L plane which equalizes θ_s and θ_R . This component is therefore orthogonal to N_{d1} and is directed along

$$N_{d2} = \pm (L \times n). \quad (5.11)$$

Here the appropriate sign is determined as follows:

$$\begin{array}{l}
 \text{Positive} \\
 \text{Negative}
 \end{array}
 \left\{ \begin{array}{l}
 \theta_S > \theta_R \text{ and condition (5.5a) is true;} \\
 \theta_S < \theta_R \text{ and condition (5.5b) is true.} \\
 \\
 \theta_S > \theta_R \text{ and condition (5.5b) is true;} \\
 \theta_S < \theta_R \text{ and condition (5.5a) is true.}
 \end{array} \right.$$

5.4 Pitch Control During Momentum Alignment

It is necessary to control the pitch during momentum alignment for the following three reasons:

- (i) An impulsive disturbance significantly affecting $\dot{\lambda}$ (pitch rate) produces a deviation far out of proportion to maximum roll-yaw divergence.
- (ii) Pitch rate is in part governed by the projection of L on the symmetry axis L_x . As L is moved, changing θ_S , the projection given by $L_x = |L \cos \theta_S|$ also changes. Therefore roll-yaw control has a direct influence on the pitch rate, often leading to pitch divergence.
- (iii) Since the precession rate ψ depends strongly on the magnitude of L , increasing $|L|$ to off-set the reduction of L_x in condition (ii) at large θ_S also serves to speed alignment.

The third moment component N_{d3} is orthogonal to both N_{d1} and N_{d2} in order to minimize interference with alignment during pitch control. Thus N_{d3} must align with L , changing only its magnitude.

This phase of the pitch control operates on a quasi bang-bang fashion and is somewhat less refined than the final pitch alignment. Initially

the pitch deviation $\Delta\lambda = \lambda - \lambda_f$ is determined. The pitch control is then effected if:

- (i) $|\Delta\lambda| > 0$, indicating misalignment; and/or
- (ii) $|\dot{\lambda}| > 0$, implying drift from alignment.

In case of condition (i), a bang-bang switch point is set, $\Delta\lambda_s = \Delta\lambda/1.8$. For $\Delta\lambda < \Delta\lambda_s$, $|L|$ is increased; while for $\Delta\lambda > \Delta\lambda_s$, L is decreased. $\Delta\lambda_s$ is reset when $\dot{\lambda}$ passes through zero, and $|\dot{\lambda}|$ is maintained within fixed bounds to prevent the change in $|L|$ substantially influencing roll-yaw control. In case of condition (ii), $|L|$ is reduced for $\dot{\lambda} > 0$ and vice versa.

These changes in $|L|$ are produced by providing a third moment component N_{d3} directed along L ,

$$N_{d3} = \pm \frac{L}{|L|} . \quad (5.12)$$

The pitch control strategy described above has been quite simplified. The precession rate $\dot{\psi}$, is strongly influenced by large increases or decreases in $|L|$. Consequently, the roll-yaw strategy would be affected adversely if $|L|$ were allowed to change without bound. Hence it was found that pitch and roll-yaw could be favourably balanced if pitch control maintained a bound on $\dot{\lambda}$ (which directly affects $|L|$),

$$32^\circ < |\dot{\lambda}| < 270^\circ \text{ per orbit} . \quad (5.13)$$

It was also necessary to specify an orbit tolerance so that $\Delta\lambda$ attains zero within

$$18^\circ < |\Delta\theta| < 30^\circ . \quad (5.14)$$

Thus, $|L|$ is increased if:

- (i) $\Delta\lambda < \Delta\lambda_s$ and $\dot{\lambda}$ is within bound (5.13). This brings $\Delta\lambda$ to zero within orbital tolerance (5.14).
- (ii) $\Delta\lambda = 0$ but $\dot{\lambda} < 0$.
- (iii) The absolute lower limit of condition in (5.13) is violated.

$|L|$ is decreased if:

- (i) $\Delta\lambda > \Delta\lambda_s$ and $\dot{\lambda}$ is within bound (5.13). This brings $\Delta\lambda$ to zero within orbital tolerance (5.14).
- (ii) $\Delta\lambda = 0$ but $\dot{\lambda} > 0$.
- (iii) The absolute upper limit of condition in (5.13) is violated.

Retaining N_{d3} as a unit vector as opposed to a vector of finite magnitude, was found to produce unsatisfactory results. In fact, it was necessary at times to increase N_{d3} upto three units over N_{d1} and N_{d2} . The degree of increase was determined by two factors:

- (i) Whether θ_s is increasing or decreasing.

This is because an increase of θ_s causes an increase in the angular momentum component L_x without the aid of N_{d3} and vice versa.

- (ii) Whether the past action on $|L|$ had the desired effect on $\dot{\lambda}$.

That is, if $\dot{\lambda}$ increased when it is required to increase or vice versa.

The three unit limit was imposed because the increase of N_{d3} also has the effect of slowing roll-yaw control.

5.5 Total Applied Moment

The final resultant moment direction is obtained as

$$\mathbf{N}_d = \mathbf{N}_{d1} + \mathbf{N}_{d2} + \mathbf{N}_{d3} . \quad (5.15)$$

Though no optimal control studies were done on roll-yaw alignment, it is expected that the bang-bang nature of the control with maximum moment would approximate a time optimal strategy. This was substantiated by the symmetry of the convergence and divergence trajectories of the response to typical disturbances. Furthermore, it should be pointed out that the strategy incorporates the attractive feature of having no controller gains to be optimized.

5.6 Final Pitch Alignment

Once momentum alignment (roll-yaw alignment) has been achieved, the control strategy switches to the path on the right in Figure 5.2 for final pitch control phase. First λ must be driven to zero. Since \mathbf{L} and \mathbf{I}_s are aligned, the entire controller power can now be concentrated to damp the pitch motion by applying moments along \mathbf{L} in the manner:

$$\dot{\lambda} \quad \left\{ \begin{array}{l} > 0, \mathbf{N}_d = -\mathbf{L} ; \\ < 0, \mathbf{N}_d = \mathbf{L} . \end{array} \right. \quad (5.16a)$$

$$(5.16b)$$

At the final decision point ($\lambda = \lambda_f ?$) where $\dot{\lambda}$ is effectively zero, there is no guarantee that the pitch angle is properly aligned. Thus, the objective

is to achieve pitch alignment as quickly as possible.

It is obvious that for pitch alignment the control moments are applied in a direction along the symmetry axis. Since the satellite is aligned with the orbit normal (I_s normal to the orbit), the maximum moments in opposite directions are equal. Therefore, a time optimal bang-bang control strategy may be employed.

Thus, final pitch control consists of setting a λ switch point (λ_s) and then driving the system at the maximum power with the moment directed along the symmetry axis I_s . When the switch point is crossed, the moment direction is reversed until $\dot{\lambda} = 0$ whereupon a new set point is specified. This process is repeated until $\lambda = \lambda_f$. Table 5.1 indicates choice of the switch point (λ_s) and the corresponding moment direction according to the initial conditions each time $\dot{\lambda}$ passes through zero.

Table 5.1 Switch point and moment direction during final pitch alignment.

CONDITIONS AS λ PASSES ZERO	SWITCH POINT (λ_s)	APPLIED MOMENT DIRECTION
$\lambda_f < \lambda_o$ and $\lambda_o - \lambda_f < \Pi$	$\lambda_s = \frac{k(\lambda_o + \lambda_f)}{2}$	$N_d = -I_s$
$\lambda_f < \lambda_o$ and $\lambda_o - \lambda_f \geq \Pi$	$\lambda_s = \frac{k(\lambda_o + \lambda_f + 2\Pi)}{2}$	$N_d = I_s$
$\lambda_f > \lambda_o$ and $\lambda_o - \lambda_f < \Pi$	$\lambda_s = \frac{k(\lambda_o + \lambda_f)}{2}$	$N_d = I_s$
$\lambda_f > \lambda_o$ and $\lambda_o - \lambda_f \geq \Pi$	$\lambda_s = \frac{k(\lambda_o + \lambda_f - 2\Pi)}{2}$	$N_d = -I_s$

On completion of a bang-bang control cycle, it may still be possible that

pitch alignment is not achieved, i.e., $\lambda \neq \lambda_f$. This may be attributed to an imbalance in moments, caused by friction effects, acting before and after the switch point. This is compensated by skewing the switch point through k , which is initially taken as unity and reset after each successive trial as

$$k = k_{\text{old}} \frac{\text{expected } \lambda \text{ throw}}{\text{actual } \lambda \text{ throw}} .$$

The principles underlying this form of compensation are presented in Appendix C.

5.7 Arbitrary Orientation in Space

The control strategy was devised about the premise that the final alignment position is stable. Thus, the orientation of the spacecraft specified by L_R was not only an equilibrium point but also a fixed direction for any position in the orbit. When I_s and L are aligned with L_R , the satellite remains in that position unless disturbed. However, for general γ_f and β_f , L_R does not remain fixed in space. Thus I_s remains aligned with L_R only if a control moment is continuously applied throughout the orbit. In such a case, we would require the controller to maintain I_s aligned with L_R without also aligning L . L is positioned at some optimal angle θ_s so that I_s is capable of keeping up with the progression of L_R . This is obviously quite an involved procedure and hence several extensions were added to the basic control strategy devised earlier. They are:

- (i) If $|\theta_s - \theta_R| > \theta_g/2$, when not in Phase 1 (Part 1) where θ_g is diverging, suspend application of N_{d1} and act to equalise θ_s and θ_R . This condition occurs during first repositioning of the satellite from a stable position, or when maintenance of $\theta_s = \theta_R$ is particularly difficult.

- (ii) When condition (i) is in effect, restrict \mathbf{N}_{d3} to one unit in magnitude in order not to slow the equalization.
- (iii) In Phase 1 (Part 2), continually reset θ_{g0} . This indicates that \mathbf{L}_R is separating from \mathbf{I}_S faster than the precession rate. θ_g will presumably begin to decrease at approximately the optimal value of θ_S for arbitrary orientation placement.
- (iv) If θ_g increases while in Phase 2, then the precession rate is too slow (θ_S too small) and convergence cannot occur. Therefore Phase 1 (Part 2) must be re-entered and θ_{g0} reset until θ_g begins to decrease again.
- (v) If \mathbf{I}_S overtakes \mathbf{L}_R and the control enters Phase 1 (Part 1), two conditions are examined for and acted upon:
 - (a) If θ_g is less than some specified tolerance then it is assumed that the precession rate is marginally too fast, and can be reduced by reducing θ_S and θ_R . This would cause \mathbf{L}_R to overtake \mathbf{I}_S later, placing the control back into Phase 1 (Part 2). To facilitate this action no equalization moments \mathbf{N}_{d2} are applied since these would slow and probably destabilize the control.
 - (b) If the angle between the n - \mathbf{L} plane and the \mathbf{I}_S - \mathbf{L}_R plane is less than 60° , it is likely to be easier and quicker to turn \mathbf{L} sideways using \mathbf{N}_{d2} , through the \mathbf{I}_S - \mathbf{L}_R plane, to enter Part 2 than to remain in Part 1 and simply decrease θ_S and θ_R . This speeds up implementation of the control and prevents divergence in certain situations after \mathbf{I}_S overtakes \mathbf{L}_R .
- (vi) It was found that the maximum increase in θ_S must be constrained more sharply than during stabilization control. Previously θ_S was limited to less than 80° . In the case of arbitrary orientation it was found necessary to limit θ_S to about 50° . Larger values of θ_S led to underdamped response

with poor convergence. Determination of the optimal θ_s limit for a particular final position can be achieved only through a trial and error approach.

- (vii) After reducing θ_s as required in (vi), if θ_g is still found to be greater than the Phase 1-Phase 2 switch point, the control holds L in station at the critical θ_s . This speeds I_s and L_R convergence and provides an opportunity to stabilize pitch.

The procedure is amenable to further refinement though the proposed extensions do lead to generally effective and stable control.

6. RESULTS AND DISCUSSIONS

Effectiveness of the controller is demonstrated through two configurations representing current trends in communications satellite technology.

INSAT-1A is about 20 m long from the end of the solar array to the tip of the solar sail and weighs 1,089 kg (Figure 1.2). The main body is 2.18 x 1.55 x 1.42 m. In the simulation, a value of 80 is assigned to the controller dynamics parameter which corresponds to the plate area of 2.5 m² and the moment arms of 12.2 m. The original configuration was slightly modified by the addition of a boom as a mount for the second control flap. Thus the inertia ratio for uncontrolled motion is $I=0.3$ whereas for controlled motion it has a value of 0.2. A controller offset ratio of $h/\epsilon=2$ was chosen.

L-SAT 1 has an array span of 33 m and a payload mass of 600 kg (Figure 1.3). The body dimensions are 3.5 x 2.1 x 1.75 m. A plate area of 2.5 m² and moment arms of 16 m give a controller dynamics parameter of $C=10$. Once again the inertia parameter was taken as $I=0.2$ and the offset ratio was set as $h/\epsilon=2$.

The system involves a large number of parameters associated with the orbital elements, satellite geometry and inertia, solar information and controller configuration. The results presented here attempt to assess the significance of their influence on the spacecraft's librational dynamics.

For nominal orientation control, each satellite was given a large impulsive disturbance corresponding to micrometeorite bombardment over a 24 hour period, i.e., $-0.05 < \gamma'_0, \beta'_0, \lambda'_0 < 0.05$. This corresponds to the initial librational velocity of 0.05 radians per radian of the orbital motion. The final tolerance demanded by the controller was 5×10^{-5} radians. The numerical integration step-size was reduced adaptively during execution from a base step size of 0.05° for L-SAT

and 0.025° for **INSAT 1-A**. The controller's effectiveness was evaluated against the standard pointing accuracy requirement of 0.01°

Figures 6.1 and 6.2, summarise the effect of orbital inclination on the controller's effectiveness. As can be expected, in the absence of any control, both the satellites become unstable rather quickly (Figures 6.1a, 6.2a). However, note the effectiveness of the solar pressure based control strategy. It is able to damp such a severe disturbance in a fraction of an orbit! The maximum amplitude attained is also quite small. This is particularly true in the case of **INSAT 1-A** where the maximum amplitudes in roll and yaw are approximately 4×10^{-3} degree. Such a near optimum performance of the solar controller is one to two orders of magnitude better than that reported by Modi et al.^{9-13,17-19} Effectiveness of the controller over the wide range of orbit inclinations promises applications in a variety of missions.

Figures 6.3 and 6.4 present the performance of the controller in orbits of differing eccentricity. The controller continues to be effective even in the presence of eccentricity induced librations in addition to the external impulsive disturbance! Note, the principal influence of a noncircular orbit is to increase the control period and the maximum amplitudes of librations.

The influence of the solar aspect angle ϕ is shown in Figures 6.5 and 6.6. ϕ is a measure of the orientation of the satellite's orbit relative to the Earth-Sun line. It is seen that the influence of ϕ is quite small, affecting primarily the roll and yaw, indicating near independence of the time of year at which a disturbance is applied.

Performance of the solar pressure controller is quite dependent upon the Sun's activity, eclipse and passage through Earth's shadow. Their influence is primarily reflected in the value of C through a change in the solar pressure intensity. Figure 6.7 studies controller's performance over a range of C to account for such situations. It is indeed gratifying that the controller's performance remains entirely

untarnished. As expected, larger values of C lead to a more damped response.

Finally, Figure 6.8 explores the possibility of undertaking large angle maneuvers using such a semi-passive controller. The controller is commanded to impart **L-SAT 1** a new orientation with respect to the original equilibrium configuration through roll, yaw and pitch rotations of 40° , -20° and 45° , respectively. It appears that the final configuration is acquired in about one to two orbits. This freedom to position a satellite in different orientations would enable it to undertake diverse missions.

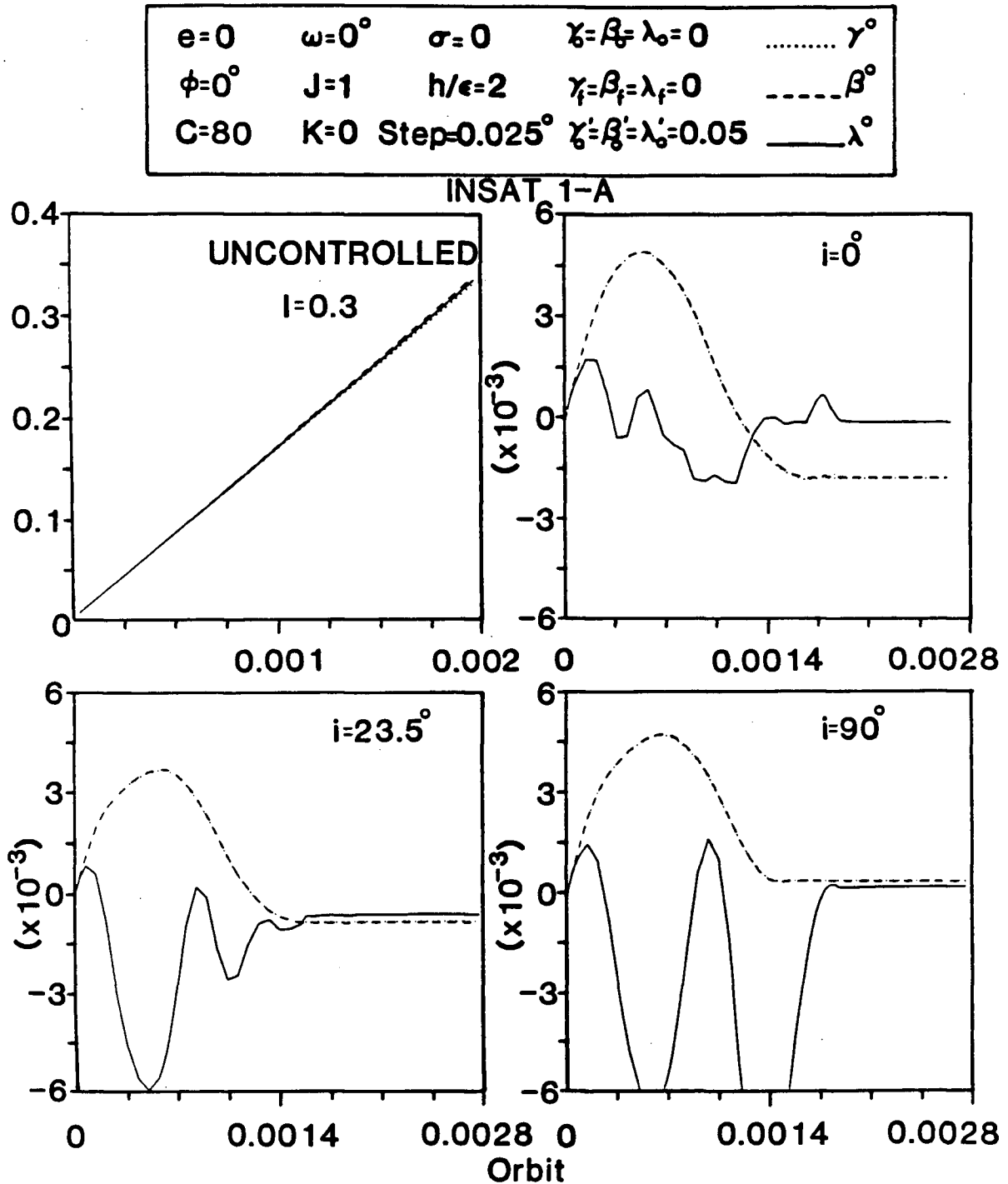


Figure 6.1

Librational response of INSAT 1-A to a representative impulsive disturbance in an ecliptic orbit in the uncontrolled mode and in orbits of varying inclinations in the controlled mode.

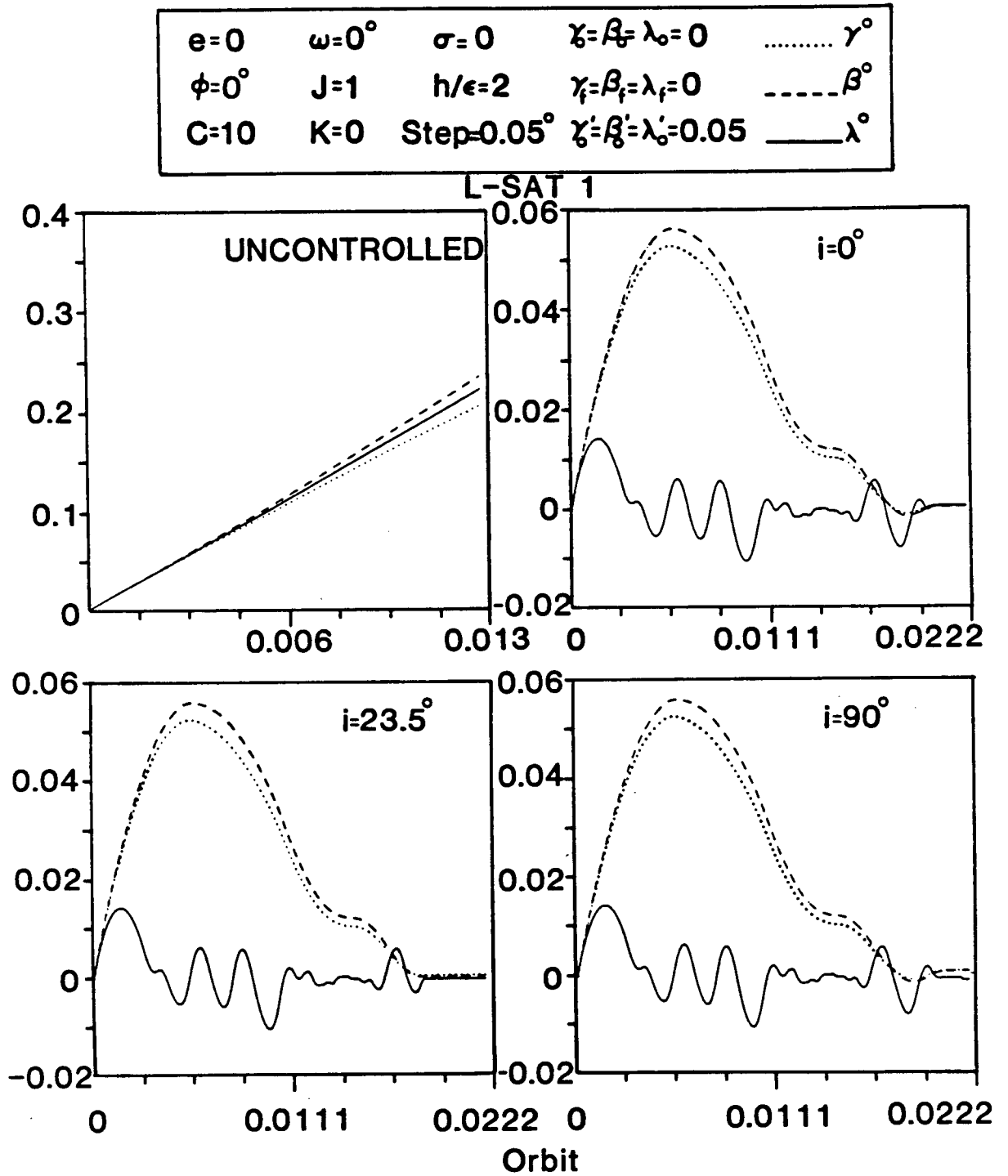


Figure 6.2

Librational response of L-SAT 1 to a representative impulsive disturbance in an ecliptic orbit in the uncontrolled mode and in orbits of varying inclinations in the controlled mode.

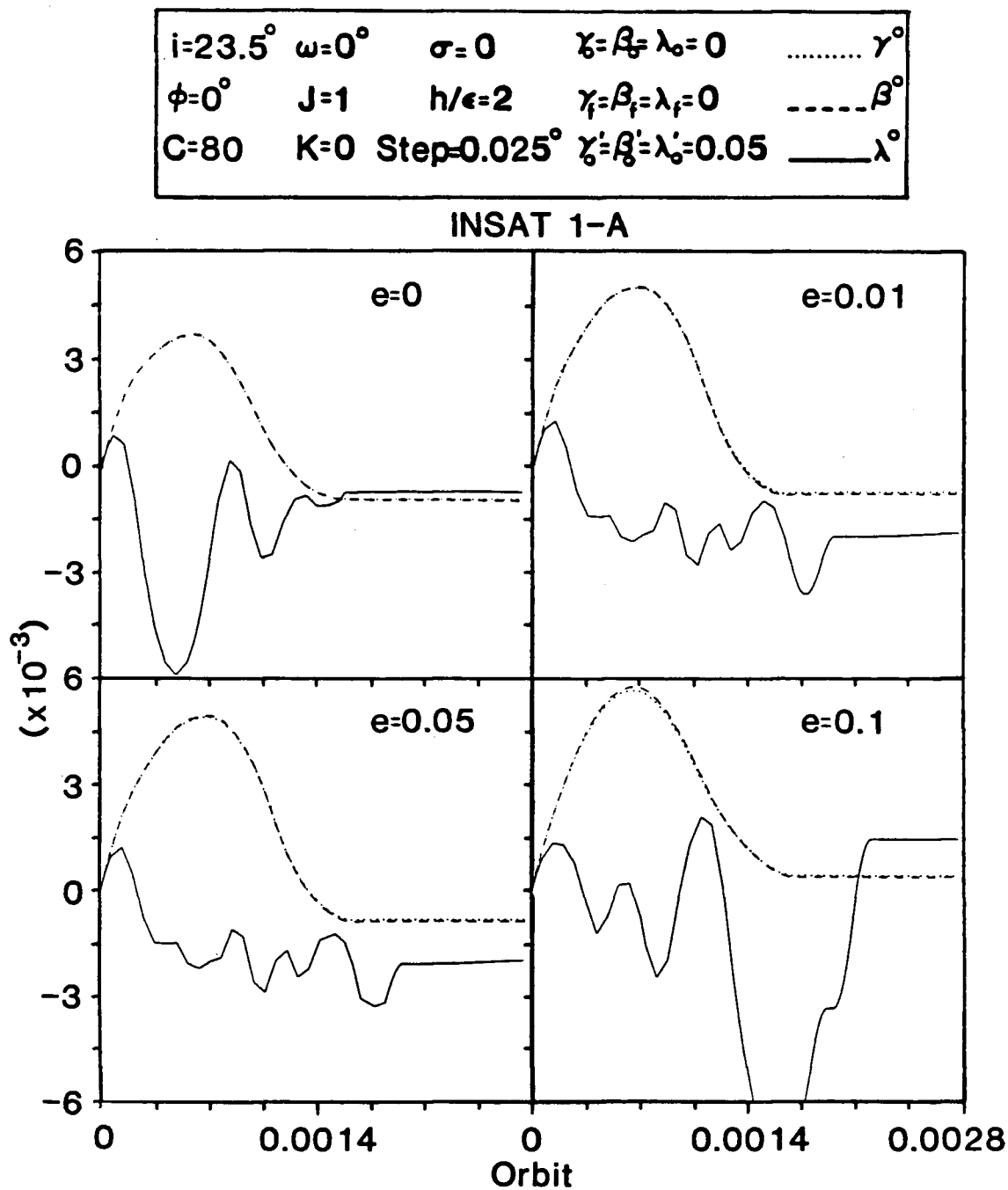


Figure 6.3

Effectiveness of the near-optimal solar pressure control strategy on INSAT 1-A for elliptic orbits.

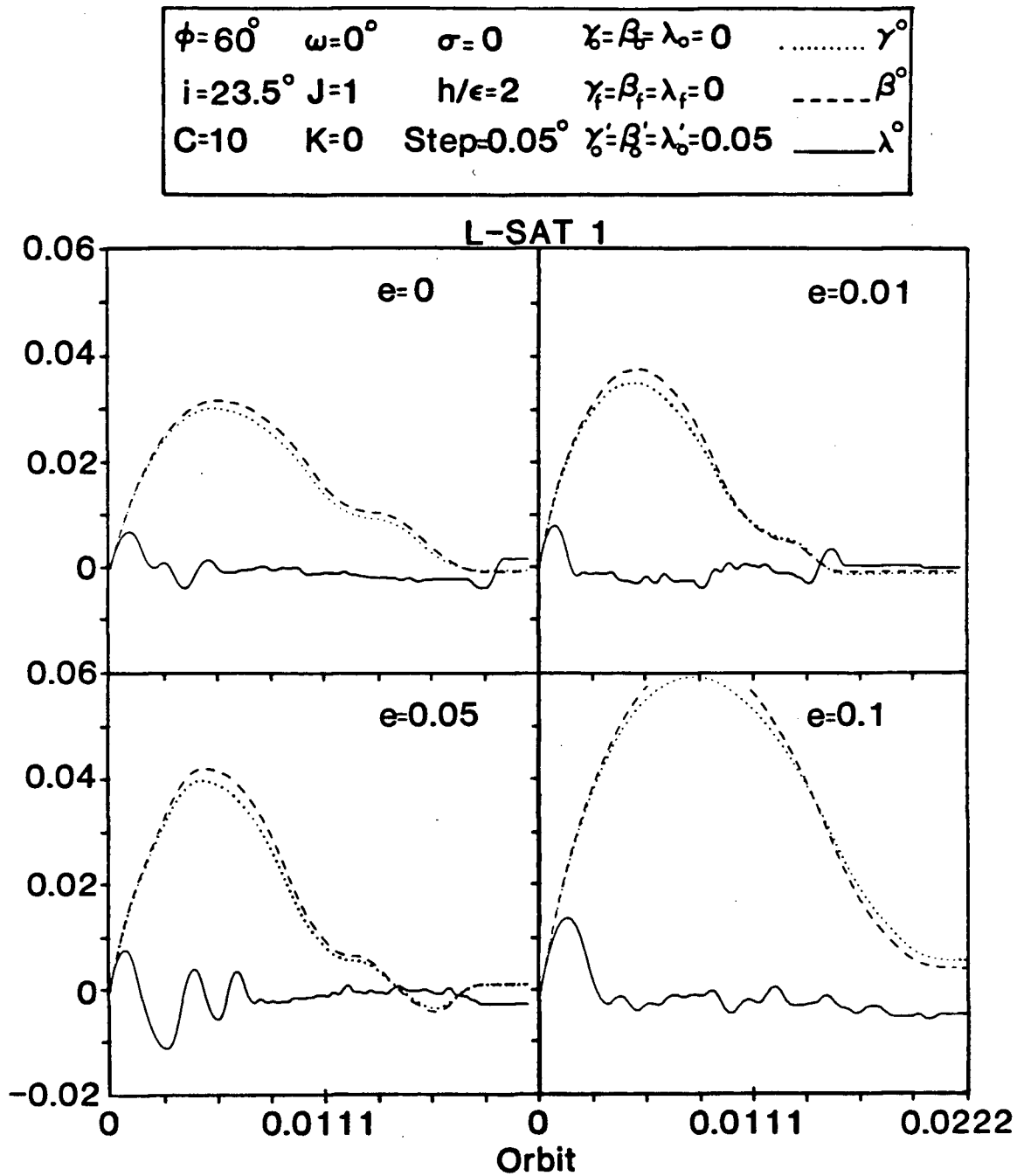


Figure 6.4 Influence of varying orbit eccentricities on the controlled librational response of L-SAT 1.

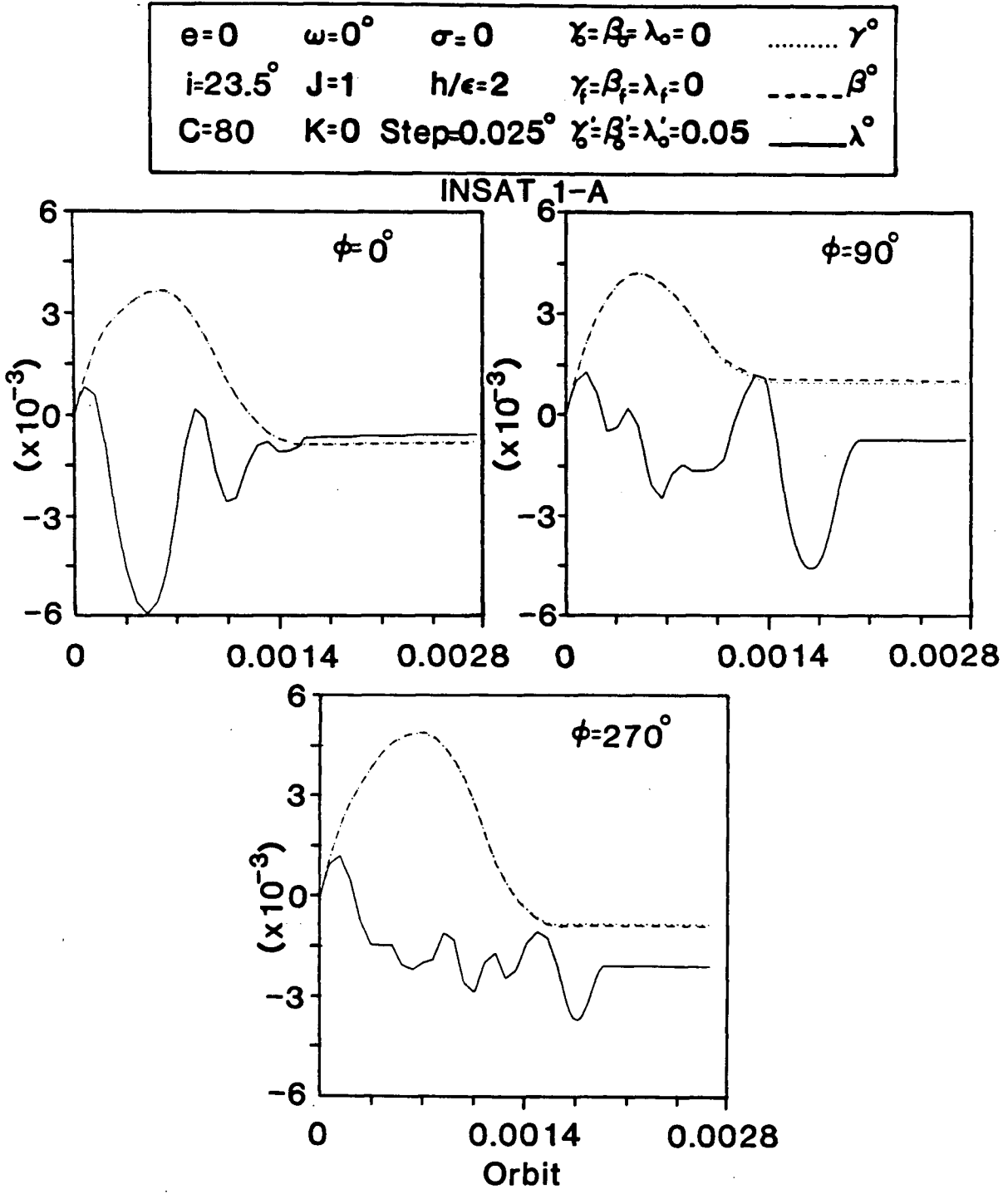


Figure 6.5

Effect of solar aspect angle on the attitude motion of INSAT 1-A with the solar pressure controller.

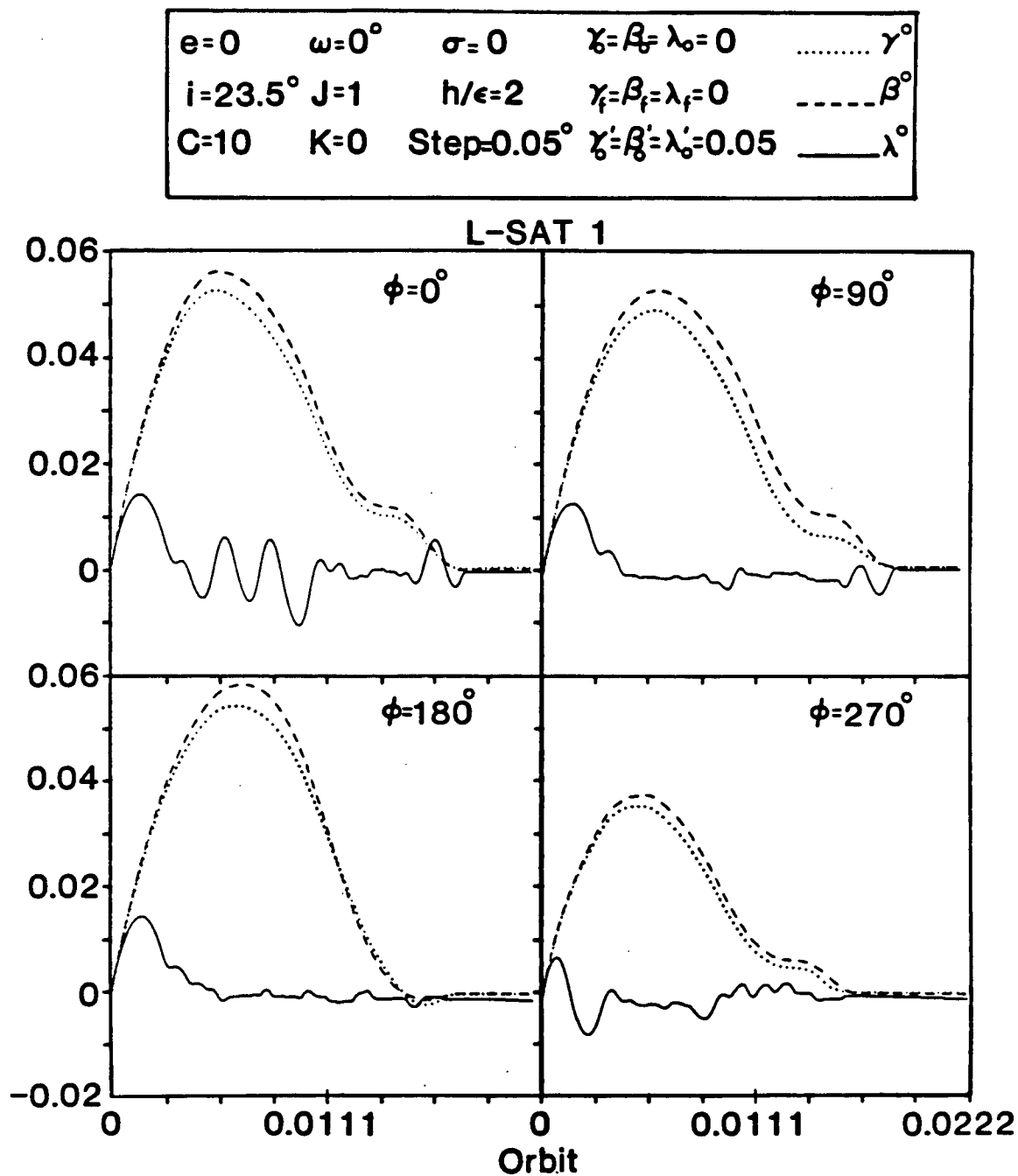


Figure 6.6

Influence of varying solar aspect angles on the librational response of L-SAT 1 in the presence of the solar pressure controller.

$e=0$	$\omega=0^\circ$	$\sigma=0$	$\zeta=\beta_f=\lambda_o=0$ γ°
$\phi=0^\circ$	$J=1$	$h/\epsilon=2$	$\chi_f=\beta_f=\lambda_f=0$	----- β°
$i=23.5^\circ$	$K=0$	$\text{Step}=0.05^\circ$	$\zeta_f=\beta_f=\lambda_o=0.05$	—— λ°

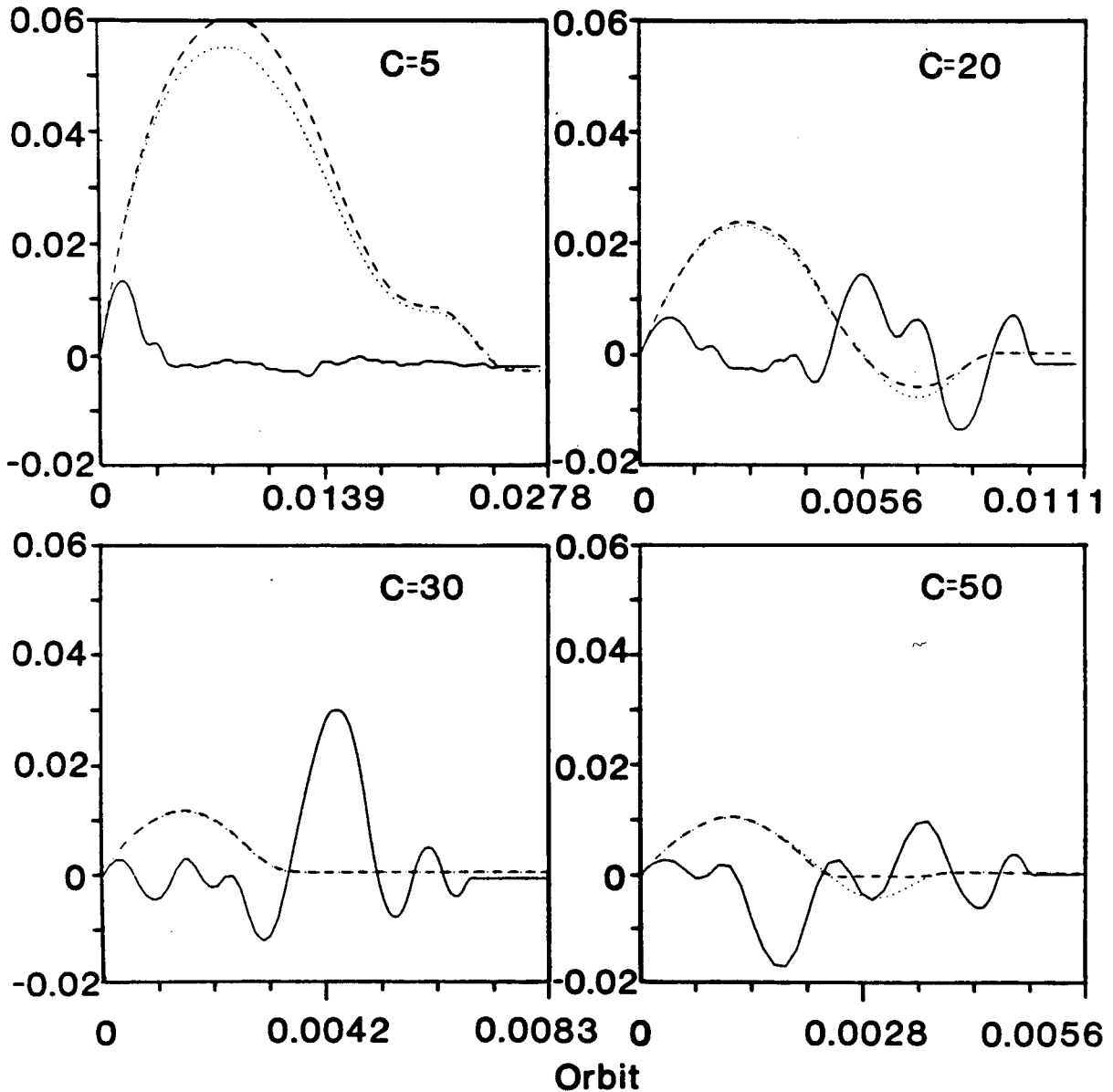


Figure 6.7 Effect of changes in the controller dynamics parameter on the librational response.

$e=0$	$C=80$	$\sigma=0$	$\text{Step}=0.05^\circ$ γ°
$\phi=0^\circ$	$J=1$	$h/\epsilon=2$	$\gamma_0=\beta_0=\lambda_0=0$	----- β°
$i=23.5^\circ$	$K=0$	$\omega=0^\circ$	$\gamma'_0=\beta'_0=\lambda'_0=0$	——— λ°

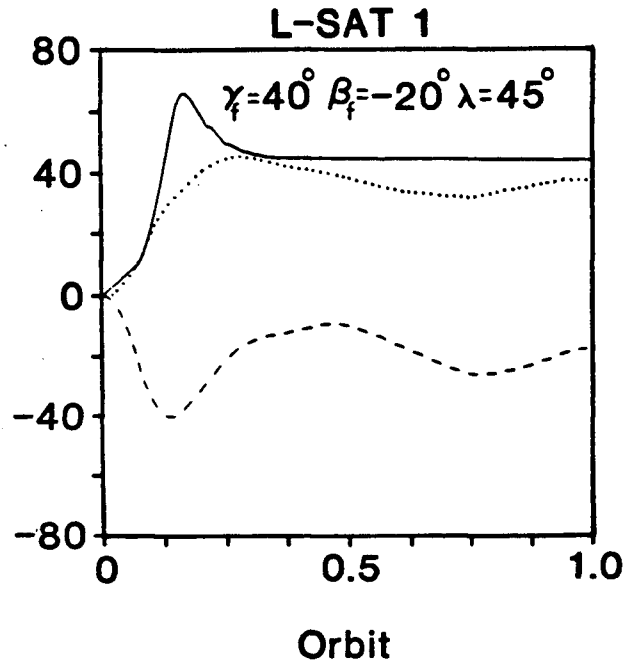


Figure 6.8

Plot showing versatility of the solar pressure controller in undertaking large angle slewing maneuvers.

7. CONCLUDING REMARKS

The analysis suggests that the solar pressure control strategy originally proposed by Lunscher and Modi appears to remain effective over a wide range of system parameters, solar activity and Earth's shadow. In particular, it is quite successful in damping exceedingly severe disturbance induced librations of large communications satellites launched recently (**INSAT 1-A**) or currently being designed (**L-SAT 1**). The solar pressure can also be used to undertake large angle slewing maneuvers. The semi-passive character of the controller promises a longer lifespan for satellites thus making them more cost-effective.

It might be appropriate to suggest at this stage a course of future research that is likely to be fruitful. There are several areas in which the model presented could be improved:

- (i) The strategy for arbitrary orientation of the satellite may be modified so that it is time-optimal or more explicitly determines the optimal θ_s .
- (ii) Flexibility effects of the solar panels for larger satellites should be incorporated in the dynamical relations as well as in the controller's generalized forces.
- (iii) Utilization of the solar radiation pressure based control strategy for station-keeping in an orbital drift situation may prove to be profitable.
- (iv) Effect of the Earth's albedo and scattered radiation from the Earth's atmosphere should be considered in a more sophisticated model.
- (v) It may be possible to determine the minimum grid resolution for storage to obtain adequate accuracy. In such a case, the optimization algorithms need not be executed on board the satellite as only reference to a stored table of predetermined plate rotations would be required.

LIST OF REFERENCES

1. Moran, J.P., "Effects of Plane Librations on the Orbital Motion of Dumbbell Satellite", *ARS Journal*, Vol. 31, No. 8, August 1961, pp. 1089-1096.
2. Yu, E.Y., "Long-Term Coupling Effects Between the Librational and Orbital Motions of a Satellite", *AIAA Journal*, Vol. 2, No. 3, March 1964, pp. 553-555.
3. Shrivastava, S.K., and Modi, V.J., "Satellite Attitude Dynamics and Control in the Presence of Environmental Torques- A Brief Review", *Journal of Guidance, Control and Dynamics*, Vol.6, No.6, Nov.-Dec. 1983, pp. 461-471.
4. Brereton, R.C., "A Stability Study of Gravity Oriented Satellites", Ph.d. Thesis, Department of Mechanical Engineering, University of British Columbia, September 1967.
5. Roberson, R.E., "Attitude Control of a Satellite Vehicle -An Outline of the Problem", *Proceedings of VIII International Astronautical Congress, International Astronautical Federation*, Paris, 1958, pp. 317-339.
6. Garwin, R.L., "Solar Sailing - A Practical Method of Propulsion Within the Solar System", *Jet Propulsion*, Vol. 28, 1958, pp. 188-190.
7. Sohn, R.L., "Attitude Stabilization by means of Solar Radiation Pressure", *ARS Journal*, Vol. 29, 1959, pp. 371-373.
8. Hibbard, R.R., "Attitude Stabilization using Focused Radiation Pressure," *ARS Journal*, Vol. 31, 1969, pp. 844-845.

9. Flanagan, R.C., and Modi, V.J., "Attitude Dynamics of a Gravity-Oriented Satellite Under the Influence of Solar Radiation Pressure", *Aeronautical Journal*, Vol.74, 1970, pp. 835-841.
10. Modi, V.J., and Flanagan, R.C., "Librational Damping of a Gravity Oriented System Using Solar Radiation Pressure", *Aeronautical Journal*, Royal Aeronautical Society, Vol. 75, August 1971, pp. 560-564.
11. Modi, V.J., and Kumar, K., "Librational Dynamics of Gravity-Oriented Satellite Under the Influence of Solar Radiation Pressure", *Proceedings of International Symposium on Computer Aided Engineering*, Waterloo, 1971, pp. 359-37.
12. Modi, V.J. and Kumar, K., "Coupled Librational Dynamics and Attitude Control of Satellites in Presence of Solar Radiation Pressure", *Astronautical Research*, D.Reidel Publishing Co., 1971, pp. 37-52.
13. Modi, V.J., and Pande, K.C., "Solar Pressure Induced Librations of Spinning Axisymmetrical Satellites", *Journal of Spacecraft and Rockets*, Vol.10, 1973, pp. 615-617.
14. Shrivastava, S.K., and Hablani, H.B., "Analysis of Solar Radiation Pressure Induced Coupled Librations of Gravity-Stabilized Axisymmetric Satellites", *Celestial Mechanics*, Vol.20, 1979, pp. 297-313.
15. Galitiskaya, E.B., and Kisler, M.I., "Radiation Control of the Orientation of Space Probes", *Cosmic Research*, Vol.3, 1965, pp. 298-301.

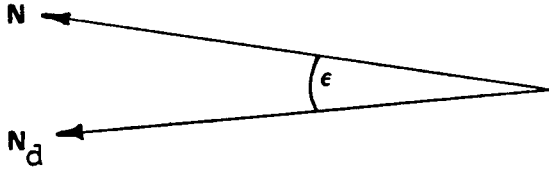
16. Scull, J.R., "Mariner IV Revisited - or the Tale of the Ancient Mariner", Paper No.27, *XX International Astronautical Congress, Mar del Plata, Argentina, 1969.*
17. Modi, V.J., and Pande, K.C., "Solar Pressure Control of a Dual Spin Satellite", *Journal of Spacecraft and Rockets, Vol.10, 1973, pp. 355-361.*
18. Modi, V.J., and Pande, K.C., "A Bang-Bang Solar Pressure Attitude Control System", *Journal of the Aeronautical Sciences, Vol. XXII, No. 1, July - Sept. 1974, pp. 1-20.*
19. Lunscher, W.H.H.J., and Modi, V.J., "A Strategy for Three-Axis Librational Control of Spacecraft Using Solar Pressure", *AIAA/AAS Astrodynamics Conference, San Diego, California, August 1982, Paper No. 82-1417.*
20. U.B.C. DE, "Solution of Ordinary Differential Equations with Refined Error Control", *U.B.C. Computing Center, Vancouver, Canada.*
21. Shampine, L.F., and Gordon, M.K., *Computer Solution of Ordinary Differential Equations: The Initial Value Problem, Freeman, 1974.*
22. Luenberger, D.G., *Introduction to Linear and Nonlinear Programming, Addison-Wesley Publishing Company, 1973.*
23. Meirovitch, L., *Methods of Analytical Dynamics, McGraw-Hill Book Company, 1970.*

APPENDIX A: EVALUATION OF $g_{1x} \Big|_{\epsilon=0}$

The directional constraint g_1 was defined as,

$$g_1 = \left[2 \left\{ 1 - \frac{\mathbf{N} \cdot \mathbf{N}_d}{|\mathbf{N}| |\mathbf{N}_d|} \right\} \right]^{1/2}. \quad (\text{A.1})$$

The reasoning underlying this constraint is readily apparent from the vector diagram below,



Since $\frac{\mathbf{N} \cdot \mathbf{N}_d}{|\mathbf{N}| |\mathbf{N}_d|} = \cos \epsilon$, g_1 becomes zero when the vectors are aligned

with $\epsilon = 0$. Furthermore, since

$$\cos \epsilon \approx \left(1 - \frac{\epsilon^2}{2} \right), \quad \epsilon \ll 1, \quad (\text{A.2})$$

$g_1 \approx \epsilon$ near alignment.

The gradient of g_1 is evaluated as follows:

$$\begin{aligned} g_{1x} &= \left[2 \left\{ 1 - \frac{\mathbf{N} \cdot \mathbf{N}_d}{|\mathbf{N}| |\mathbf{N}_d|} \right\} \right]^{-1/2} \left(\frac{\mathbf{N} \cdot \mathbf{N}_d}{|\mathbf{N}| |\mathbf{N}_d|} \right)_x \\ &= - (g_1 |\mathbf{N}| |\mathbf{N}_d|)^{-1} \left[\mathbf{N}'_x \mathbf{N}_d - \frac{(\mathbf{N} \cdot \mathbf{N}_d)}{|\mathbf{N}|^2} \mathbf{N}'_x \mathbf{N} \right] \\ &= - (g_1 |\mathbf{N}| |\mathbf{N}_d|)^{-1} \mathbf{N}'_x \left[\mathbf{N}_d - \frac{(\mathbf{N} \cdot \mathbf{N}_d)}{|\mathbf{N}|^2} \mathbf{N} \right] \end{aligned}$$

$$= - (g_1 |N| |N_d|)^{-1} N'_x \left[N_d - (\hat{N} \cdot N_d) \hat{N} \right]. \quad (\text{A.3})$$

At $g_1 \approx 0$, $\hat{N} \cdot \hat{N}_d \approx 1$, hence

$$g_{1x} \Big|_{\epsilon=0} = \frac{N'_x}{g_1 |N|} [\hat{N} - \hat{N}_d] ;$$

but at $g_1 = 0$, $\hat{N} = \hat{N}_d$, hence

$$g_{1x} \Big|_{\epsilon=0} = \frac{N'_x}{|N|} \frac{0}{0} .$$

To understand this singularity let us apply L' Hospitals' rule with respect to the separation angle ϵ . Since near alignment $g_1 \approx \epsilon$,

$$\lim_{\epsilon \rightarrow 0} \frac{dg_1}{d\epsilon} = 1 .$$

Also, in general,

$$\frac{d}{d\epsilon} (\hat{N} - \hat{N}_d) = \frac{d\hat{N}}{d\epsilon} , \quad (\text{A.4})$$

therefore at alignment,

$$g_{1x} \Big|_{\epsilon=0} = \frac{N'_x}{|N|} \frac{d\hat{N}}{d\epsilon} . \quad (\text{A.5})$$

However, the derivative in equation (A.4) represents a unit vector pointing in the direction from which the vector is approaching alignment. As such, the gradient of g_1 on alignment depends on the path N followed to achieve alignment. Therefore $g_{1x} \Big|_{\epsilon=0}$ is not an analytic function, rendering it undefined.

To illustrate, suppose $N_d = i$ and N is approaching alignment from the first quadrant in the x-y plane. Then

$$\mathbf{N}' = (\cos \epsilon \quad \sin \epsilon \quad 0) \quad \text{therefore}$$

$$\frac{d\mathbf{N}'}{d\epsilon} = (\sin \epsilon \quad -\cos \epsilon \quad 0), \text{ and}$$

$$\lim_{\epsilon \rightarrow 0} \frac{d\mathbf{N}'}{d\epsilon} = (0 \quad -1 \quad 0) = -\mathbf{j}.$$

$$\text{Hence } g_{1x} \Big|_{\epsilon=0} = - \frac{\mathbf{N}'_x}{|\mathbf{N}|} \mathbf{j}. \quad (\text{A.6})$$

However, if \mathbf{N} approaches alignment from the fourth quadrant of x-y plane,

$$\mathbf{N}' = (\cos \epsilon \quad \sin \epsilon \quad 0),$$

$$\lim_{\epsilon \rightarrow 0} \frac{d\mathbf{N}'}{d\epsilon} = (\sin \epsilon \quad \cos \epsilon \quad 0)_{\epsilon=0} = \mathbf{j},$$

$$g_{1x} \Big|_{\epsilon=0} = \frac{\mathbf{N}'_x}{|\mathbf{N}|} \mathbf{j}. \quad (\text{A.7})$$

Clearly equations (A.6) and (A.7) are not consistent.

APPENDIX B: CONTROL MOMENT SYMMETRIES

The locus of points generated by the endpoints of all optimal control moment vectors, \mathbf{N} , form a surface about the satellite's center of mass. It is shown here that this surface contains at least two levels of symmetry. Before proceeding, it will be noted in advance that these symmetries occur with respect to the sun-satellite line. Consequently it is convenient to normalize the solar aspect vector, \mathbf{u} , by placing it in the satellite x-y plane, ($u_z = 0$). This action, representing a simple coordinate rotation about the x-axis, does not detract from the generality of the analysis.

x-y Axis Mirror Image Symmetry

Should the satellite be physically inverted by a rotation about the z-axis while holding the controller plate rotation fixed, then the resultant moment will be a reflection of the initial moment in the x-y plane, i.e., if:

$$a_{1,f}^u = \pi - a_{1,i}^L ; \quad (\text{B.1a})$$

$$a_{1,f}^L = \pi - a_{1,i}^u ; \quad (\text{B.1b})$$

$$a_{2,f}^u = - a_{2,i}^L ; \quad (\text{B.1c})$$

$$a_{2,f}^L = - a_{2,i}^u ; \quad (\text{B.1d})$$

$$\delta_f^u = \delta_i^L ; \quad (\text{B.1e})$$

$$\delta_f^L = \delta_i^u ; \quad (\text{B.1f})$$

then by substitution of (B.1) and $u_z = 0$ into equations (3.14):

$$N_{x,f} = N_{x,j} ; \quad (B.2a)$$

$$N_{y,f} = N_{y,j} ; \quad (B.2b)$$

$$N_{z,f} = - N_{z,j} . \quad (B.2c)$$

z-axis Reflection Symmetry

If the upper and lower plate rotation α_1 and δ are turned opposite to their initial values then the resultant moments will be a reflection of the initial moments through the z-axis, i.e., if:

$$a_{1,f} = - a_{1,i} ; \quad (B.3a)$$

$$a_{2,f} = - a_{2,i} ; \quad (B.3b)$$

$$\delta_f = - \delta_i ; \quad (B.3c)$$

then

$$N_{x,f} = - N_{x,j} ; \quad (B.4a)$$

$$N_{y,f} = - N_{y,j} ; \quad (B.4b)$$

$$N_{z,f} = N_{z,j} . \quad (B.4c)$$

The above results are also obtained by substitution of (B.3) and $u_z = 0$ into equations (3.14).

When combined, the symmetries demonstrate that the optimal moment surface is fully specified by any one of the four regions bounded by the planes containing the x-y and x-z axis. Since the solar aspect vector is free to move in the

x-y plane the shape of the surface will be solely determined by its elevation angle Ω (Figures 4.1a-4.1d). When Ω is negative the physical system can be rendered identical to that of positive Ω by inversion of the satellite through a rotation about the y-axis. Consequently the moment surface produced is also simply a y-axis inversion of that produced by positive Ω . This can be considered a third form of symmetry.

APPENDIX C: BANG-BANG COMPENSATION

Pitch control is performed by a simple bang-bang control strategy with the applied moment directed along the satellite axis of symmetry. It was remarked that on completion of one control cycle, the pitch angle may not agree with that desired (λ_f). Numerous unforeseen imbalances may be responsible for this. To compensate for the imbalance, the switch point in subsequent trials was skewed by a constant proportion k . In order to determine the appropriate k the dynamics of bang-bang control in the presence of a moment imbalance is examined here.

Assume that the imbalance is due to the presence of the constant torque τ . This, for example, could correspond to frictional coupling to the rotor or plates of nonuniform reflectivity. The applied moment therefore becomes

$$\mathbf{N} = \begin{cases} T + \tau, & \lambda \leq \lambda_{sw}; \\ -T + \tau, & \lambda > \lambda_{sw}; \end{cases} \quad (\text{C.1a})$$

where λ_{sw} is set at the uncompensated bang-bang switch point,

$$\lambda_{sw} = \frac{\lambda_f + \lambda_o}{2} . \quad (\text{C.2})$$

Taking unit moment of inertia, the pitch equation of motion are:

$$\ddot{\lambda} = \mathbf{N} ; \quad (\text{C.3a})$$

$$\dot{\lambda} = \mathbf{N}t + \dot{\lambda}_o . \quad (\text{C.3b})$$

Initially, λ_o and $\dot{\lambda}_o$ are taken to be zero. Therefore the pitch rate before switching is

$$\dot{\lambda} = (T + \tau) t . \quad (C.4)$$

Equation (C.4) can be solved readily for the pitch rate at the switch point,

$$\dot{\lambda}_{sw} = [2(T + \tau) \lambda_{sw}]^{1/2} . \quad (C.5)$$

After switching the pitch rate will become zero at $\lambda_{f,2}$ at time $t_{f,2}$,

$$t_{f,2} = \dot{\lambda}_{sw} / (T - \tau) = [2(T + \tau) \lambda_{sw}]^{1/2} / (T - \tau) . \quad (C.6)$$

The stopping point is now obtained as

$$\begin{aligned} \lambda_{f,2} &= [(T + \tau) / (T - \tau) + 1] \lambda_{sw} \\ &= [(T + \tau) / (T - \tau) + 1] \lambda_f / 2 \\ &= [T / (T - \tau)] \lambda_f . \end{aligned} \quad (C.7)$$

Therefore, as expected, there is an overshoot or undershoot if $\tau \neq 0$.

If an alternate switch point is defined as

$$\lambda_{sw2} = \lambda_{f,2} / 2 , \quad (C.8)$$

and our perspective modified so that the target pitch is $\lambda_{f,2}$ instead of λ_f with switch point λ_{sw2} , then from equation (C.7):

$$\begin{aligned} \lambda_f &= [(T - \tau) / T] \lambda_{f,2} ; \\ \lambda_{sw} &= [(T - \tau) / T] \lambda_{sw2} = k \lambda_{sw2} . \end{aligned} \quad (C.9)$$

λ_{sw} is now the compensated switching angle, guaranteeing termination of control

at $\lambda_{f,2}$.

However, the underlying assumption of the control is that the magnitude of neither T nor τ is known. k can still be found if at least one trial control attempt is made using the conventional switch point equation (C.2). This provides the actual termination point $\lambda_{f,2}$, as well as that intended, λ_f . k is thus found from equation (C.7) as:

$$k = \frac{\lambda_f}{\lambda_{f,2}} = \frac{\text{expected throw}}{\text{actual throw}}. \quad (\text{C.10})$$

Equation (C.10) is only valid for the first compensated control attempt. If this does not cause pitch to align then its repeated use will produce a biased compensation constant. To remove this bias it must be recognised that the earlier analysis was founded on the expectation that the previous switch point was set at $\lambda_{sw} = \lambda_{f,2}$. Therefore,

$$\text{expected throw} = \lambda_f = 2 \lambda_{sw}.$$

However, when the switch point is compensated, λ_{sw}^c , the effective expected throw differs from the true expected throw,

$$\text{effective expected throw} = 2 \lambda_{sw}^c = 2k \lambda_{sw} = k (\text{expected throw}).$$

Therefore, the unbiased compensation constant is

$$k_{i+1} = k_i \frac{\text{expected throw}}{\text{actual throw}}, \quad (\text{C.11})$$

where $k_0 = 1$.

If an initial pitch alignment trial results in overshoot and if the perturbing force is linear and constant, then the current and next compensation constants are related by:

$$\begin{aligned}k_{i+1} + k_i &= \left(1 - \frac{\tau}{T}\right) + \left(1 + \frac{\tau}{T}\right) = 2 ; \\k_{i+1} &= 2 - k_i .\end{aligned}\tag{C.12}$$

Thus, in principle, only one trial is needed to determine the appropriate compensation. However, in practice this approach was found unsatisfactory, particularly if a great deal of overshoot was encountered in the first attempt. A separate k was therefore recorded and used for the two directions of motion, clockwise and counter-clockwise.

Control simulation found application of compensation to work marginally better than a totally uncompensated system. In practice it also proved useful to limit k to a minimum value of about 0.65. This was because the first attempt at alignment, particularly with small throws, often led to large overshoots yielding k values less than 0.5. This in turn resulted in severe overcompensation of subsequent trials, thereby slowing convergence.